NUMERICAL INVERSE SCATTERING FOR THE TODA LATTICE

DENIZ BILMAN AND THOMAS TROGDON

Abstract. We present a method to compute the inverse scattering transform (IST) for the famed Toda lattice by solving the associated Riemann–Hilbert (RH) problem numerically. Deformations for the RH problem are incorporated so that the IST can be evaulated in $\mathcal{O}(1)$ operations for arbitrarily points in the (n,t)-domain, including short- and long-time regimes. No time-stepping is required to compute the solution because (n,t) appear as parameters in the associated RH problem. The solution of the Toda lattice is computed in long-time asymptotic regions where the asymptotics are not known rigorously. We introduce two new asymptotic regions, in addition to the existing three regions, so that all values of (n,t) for t large are contained in a region. Furthermore, we define clear boundaries for all regions and develop deformations in the new regions that should be of use in future asymptotic analysis of the Toda lattice.

1. Introduction

We consider the numerical solution of the Cauchy initial value problem for the doubly-infinite Toda lattice

$$\begin{cases} \partial_t a_n(t) = a_n(t)\big(b_{n+1}(t) - b_n(t)\big) \\ \partial_t b_n(t) = 2\big(a_n(t)^2 - a_{n-1}(t)^2\big) \\ a_n(0) = a_n^0, \text{ and } b_n(0) = b_n^0, \end{cases} \tag{1}$$

for $(n,t) \in \mathbb{Z}\times\mathbb{R}$ with solutions[1] $(a(t),b(t)) \in \ell(\mathbb{Z})\times\ell(\mathbb{Z})$ satisfying

$$\sum_{n\in\mathbb{Z}} (1+|n|)^k \left(\left|a_n(t) - \tfrac{1}{2}\right| + |b_n(t)|\right) < \infty, \text{ for all } t\in\mathbb{R},\ k\in\mathbb{N}. \tag{2}$$

The Toda lattice was introduced by Morikazu Toda in [32] (see also [31]). The Toda lattice is a completely integrable model for a one-dimensional crystal. The form (1) we use in this paper is the Toda lattice written in Flaschka's variables [13]. This system has been studied in great detail because it is the prototypical discrete-space, continuous-time infinite-dimensional integrable system.

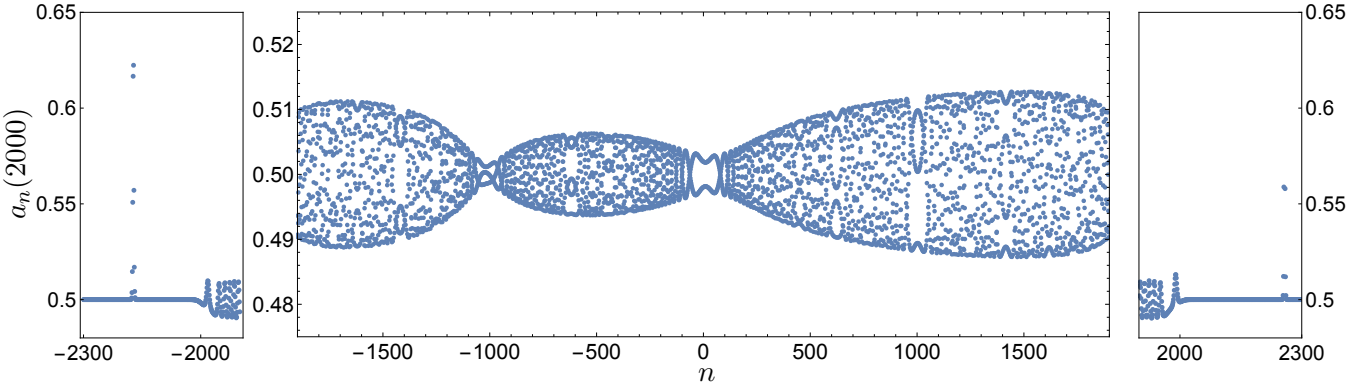

Figure 1. An example solution of the Toda lattice computed at $t = 2000$ with the method presented here. The initial data is given by $a_n(0) = 1/2 - ne^{-n^2+n}$ and $b_n(0) = n\,\mathrm{sech}\, n$. This initial data produces dispersive radiation (center panel) and four solitons, two traveling each direction (left and right panels).

The authors wish to thank Percy Deift and Irina Nenciu for useful discussions and suggestions. DB gratefully acknowledges the hospitality of Courant Institute of Mathematical Sciences, where majority of this work was done. We acknowledge the partial support of the National Science Foundation through the NSF grants DMS-1150427 (DB) and DMS-1303018 (TT). Any opinions, findings, and conclusions or recommendations expressed in this material are those of the authors and do not necessarily reflect the views of the funding sources.

[1]We omit subscripts to refer to the functions defined on $\mathbb{Z}$.

A consequence of the complete integrability of the Toda lattice is an associated inverse scattering transform (IST). The IST maps the initial data to a spectral plane where its time evolution is simple via a transformation called *direct scattering*, see Section 2.2. Then, at a given time t, the evolved spectral data is mapped back to the physical plane find the solution values $a_n(t)$ and $b_n(t)$ by a transformation called *inverse scattering*. This inverse problem is solved by considering an associated oscillatory Riemann–Hilbert (RH) problem. RH problems are boundary-value problems in the complex plane for sectionally analytic functions. General references are [2, 5, 6, 19, 33, 36, 41]. From an analytical point of view, the benefit of studying the RH problem is that asymptotics can be extracted by the method of nonlinear steepest descent. Broadly, the method works by deforming the contours of the RH problem much like contour integrals to turn oscillations to exponential decay. See [6, 9, 10] for some implementations of this method.

As for specific applications of the method of nonlinear steepest descent to the Toda lattice, we refer the reader to the work of Kamvissis [16], Krüger and Teschl [17, 18] and Teschl [29]. These works give explicit long-time asymptotics for the solution of the Toda lattice in the soliton and dispersive regions that we define in Section 2.4. The work of Kamvissis gives the asymptotic behavior in the Painlevé region (as defined in Section 2.4) for non-generic initial data.

We approach the IST from a numerical perspective. See Figure 1 for a sample solution computed with our method. Given sufficiently regular generic initial data we are able to compute the solution at any given point (n,t), to a given accuracy, in a bounded number of operations by solving the RH problem numerically and incorporating the deformations used in the method of nonlinear steepest descent. Stated another way, for any given (n,t) we give an $\mathcal{O}(1)$ algorithm to compute the two values $\{a_n(t), b_n(t)\}$. No time-stepping is required to compute these values. This methodology has been previously applied to the KdV and mKdV equations [38], the focusing and defocusing NLS equations [39], the Painlevé II equation [24, 26] and orthogonal polynomials on the line [26]. We compute the solution of the Toda lattice for arbitrarily large values of t. The complexity and the accuracy of the methodology is discussed in [27]. With the current state of the art, the use of deformations appears to be necessary as the associated RH problem is increasingly oscillatory as $|n|$ and t increase. Deformations can be avoided in some cases with oscillatory integral techniques [34] but unfortunately these methods are not currently general enough to aid in the case of the Toda lattice.

The RH problem associated with the Toda lattice has fundamental differences from problems previously solved numerically. First, the fundamental domain is the unit circle as opposed to the real axis like in the KdV, mKdV and NLS equations. Second, the RH problems in the previously solved cases have had their deformations worked out in detail. In this paper, we develop deformations for the Toda lattice in regions of the (n,t)-plane where deformations do not exist in the literature including the determination of the so-called g-function, see Appendix C. We believe our deformations will be required for future asymptotic analysis of the Toda lattice. Importantly, the asymptotic regions we define, and the deformations performed therein, cover the entire (n,t) plane. This is something, to our knowledge, that has not been performed in the literature. Finally, we encounter some interesting technical challenges in computing the functions used in the deformations, see Appendices C.3 and A. Also, in light of the work in [4] we believe this numerical method will be useful in studying non-integrable, Hamiltonian perturbations of the Toda lattice.

Due to the nonlinearity in the Toda lattice, large amplitude data induces different behavior in the solution *i.e.* a large amplitude reflection coefficient or many solitons. Large amplitude data also affects the numerical method. Throughout the manuscript, we include footnotes that highlight the complications that arise for larger initial data. Large amplitude data is a singular limit (related to small dispersion limits) and while it is of intrinsic importance, we regard it as beyond the scope of the current paper. We also do not treat the case where poles in the Riemann–Hilbert problem are very close to the unit circle. The methodology described here can be used to handle this case accurately with some extra work and deformations.

The paper is organized as follows. In Section 2 we give the background material on the IST for the Toda lattice. The direct scattering and inverse scattering maps are discussed along with a discussion of the (asymptotic) regions (soliton, dispersive, Painlevé, collisionless shock, and transition) of the Toda lattice. We also briefly discuss the numerical solution of RH problems to fix notation. The numerical computation of the scattering data, *i.e.* performing direct scattering numerically, is discussed in Section 3. The majority of the paper is devoted to Section 4 where we discuss, and explicitly derive, the deformations of the RH problem in each region. Finally, in Section 5 we give some numerical results including an error analysis. We include three appendices. Appendix A discusses the numerical solution of singular, but diagonal RH problems. Appendix B

gives a deeper discussion of computing the eigenvalues of Jacobi operators. Lastly, Appendix C details the g-function that is used in both the collisionless shock and transition regions.

2. Background material

We use this section to cover theoretical background and fix notation.

2.1. **Integrability and Lax pairs.** Complete integrability of the Toda lattice was proven by H. Flaschka in 1974 in a sequence of papers [13] and [14]. Introduce the second-order linear difference operators L and P defined on $\ell^2(\mathbb{Z})$ by

$$(Lf)_n = a_{n-1}f_{n-1} + b_n f_n + a_n f_{n+1} \tag{3}$$

$$(Pf)_n = -a_{n-1}f_{n-1} + a_n f_{n+1}\,. \tag{4}$$

and note that in the standard basis $L = L\big(\{a_n\}_{n\in\mathbb{Z}}, \{b_n\}_{n\in\mathbb{Z}}\big)$ is a Jacobi matrix (symmetric, tridiagonal with positive off-diagonals) and P is a bounded skew-adjoint operator, i.e., $P^* = -P$:

$$L = \begin{pmatrix} \ddots & \ddots & \ddots & & \\ \ddots & b_{n-1} & a_{n-1} & 0 & \\ \ddots & a_{n-1} & b_n & a_n & \ddots \\ & 0 & a_n & b_{n+1} & \ddots \\ & & \ddots & \ddots & \ddots \end{pmatrix} \quad \text{and} \quad P = \begin{pmatrix} \ddots & \ddots & \ddots & & \\ \ddots & 0 & a_{n-1} & 0 & \\ \ddots & -a_{n-1} & 0 & a_n & \ddots \\ & 0 & -a_n & 0 & \ddots \\ & & \ddots & \ddots & \ddots \end{pmatrix}.$$

The system of equations given in (1) is equivalent to

$$\partial_t L(t) = [P(t), L(t)] = P(t)L(t) - L(t)P(t), \tag{5}$$

and (P, L) is called a Lax pair and its existence shows the complete integrability of the Toda lattice. A consequence of complete integrability (or of the Lax pair) is the existence of an inverse scattering transform for the Toda lattice.

2.2. **Direct scattering: definition of the scattering data.** Since L is a bounded self-adjoint operator it bears no residual spectrum and the spectrum $\sigma(L) \subset \mathbb{R}$. Furthermore, (2) implies that the spectrum of L consists of a purely absolutely continuous part

$$\sigma_{\mathrm{ac}}(L) = [-1, 1],$$

and a finite simple pure point part

$$\sigma_{\mathrm{pp}}(L) = \{\lambda_j \colon j = 1, 2, \ldots, N\} \subset (-\infty, -1) \cup (1, +\infty)\,.$$

For convenience we map the spectrum via the Joukowski transformation:

$$\lambda = \tfrac{1}{2}\left(z + z^{-1}\right), \quad z = \lambda - \sqrt{\lambda^2 - 1}, \quad \lambda \in \mathbb{C}, \quad |z| \le 1\,.$$

Under this transformation, the a.c.-spectrum, $[-1, 1]$, gets mapped to the unit circle, $\mathbb{T}$, and the eigenvalues λ_j are mapped to $\zeta_j^{\pm 1}$, with $\zeta_j \in (-1, 0) \cup (0, 1)$ via

$$\lambda_j = \tfrac{1}{2}\left(\zeta_j + \zeta_j^{-1}\right), \tag{6}$$

for $j = 1, 2, \ldots, N$. For any z with $0 < |z| \le 1$ the problem

$$L\varphi = \frac{z + z^{-1}}{2}\varphi \tag{7}$$

has two unique solutions, φ_+ and φ_-, normalized such that

$$\lim_{n\to\pm\infty} z^{\mp n}\varphi_\pm(z; n) = 1.$$

It follows from Green's formula that the Wronskians $W\left(\varphi_\pm(z;\cdot),\varphi_\pm(z^{-1};\cdot)\right)$ are independent of n, and evaluating them at $\pm\infty$ we observe that $\{\varphi_\pm(z;\cdot),\varphi_\pm(z^{-1};\cdot)\}$ are two sets of linearly independent solutions. We define the *transmission coefficient* $T(z)$ and the *reflection coefficients* $R_\pm(z)$ by the scattering relations:

$$T(z)\varphi_+(z,n) = R_-(z)\varphi_-(z,n) + \varphi_-(z^{-1},n)$$
$$T(z)\varphi_-(z,n) = R_+(z)\varphi_+(z,n) + \varphi_+(z^{-1},n).$$

The transmission coefficient has a meromorphic extension inside the entire unit disk $|z|\leq 1$, with finitely many simple poles ζ_j, $|\zeta_j|<1$, $j=1,2,\dots,N$, which are related to the eigenvalues of L via (6). The residues of $T(z)$ are given by:

$$\operatorname*{Res}_{z=\zeta_j} T(z) = -\zeta_j\gamma_{\pm,j}\mu_j^{\mp 1},$$

where

$$\gamma_{\pm,j} = \frac{1}{\|\varphi_\pm(\zeta_j;\cdot)\|^2_{\ell^2(\mathbb{Z})}} \tag{8}$$

are the *norming constants* and μ_j is the associated proportionality constant: $\varphi_-(\zeta_j,\cdot) = \mu_j\varphi_+(\zeta_j,\cdot)$. In particular, one reflection coefficient, one set of norming constants, and the set of eigenvalues is sufficient for reconstructing L via the inverse scattering transform for Jacobi matrices whose coefficients decay sufficiently fast [30]. From this point onwards we set

$$R(z) = R_+(z) \quad \text{and} \quad \gamma_j = \gamma_{+,j}, \ \ j=1,2,\dots,N,$$

and define the set

$$\mathbf{S}(L) = \left\{R(z), \{\zeta_j\}_{j=1}^N, \{\gamma_j\}_{j=1}^N\right\} \tag{9}$$

to be the scattering data for the Lax operator L. For a more detailed account of scattering theory for Jacobi matrices, see [30] or [18].

2.3. **Inverse scattering: the Riemann–Hilbert problem.** We phrase the inverse problem in terms of a meromorphic Riemann–Hilbert problem (RH problem) $[J;\mathbb{T}]$. As in [18], we seek a function $m\colon \mathbb{C}\setminus\mathbb{T}\to\mathbb{C}^{1\times 2}$ that is meromorphic, continuous up to $\mathbb{T}$, with simple poles at $\zeta_j^{\pm 1}$, $j=1\dots,N$, and satisfies:

- *the jump condition:*

$$m^+(z;n,t) = m^-(z;n,t)J(z;n,t), \ \ z\in\mathbb{T}, \quad J(z;n,t) = \begin{pmatrix} 1-|R(z)|^2 & -\overline{R(z)}e^{-\theta(z;n,t)} \\ R(z)e^{\theta(z;n,t)} & 1\end{pmatrix},$$

- *the residue conditions:*

$$\operatorname*{Res}_{z=\zeta_j} m(z;n,t) = \lim_{z\to\zeta_j} m(z;n,t)\begin{pmatrix} 0 & 0 \\ -\zeta_j\gamma_j e^{\theta(\zeta_j;n,t)} & 0d\end{pmatrix}, \quad j=1,2,\dots,N,$$
$$\operatorname*{Res}_{z=\zeta_j^{-1}} m(z;n,t) = \lim_{z\to\zeta_j^{-1}} m(z;n,t)\begin{pmatrix} 0 & \zeta_j^{-1}\gamma_j e^{\theta(\zeta_j;n,t)} \\ 0 & 0\end{pmatrix}, \quad j=1,2,\dots,N,$$

- *the symmetry condition:*

$$m\left(z^{-1};n,t\right) = m(z;n,t)\begin{pmatrix} 0 & 1 \\ 1 & 0\end{pmatrix}, \tag{10}$$

- *the normalization condition:*

$$\lim_{z\to 0} m(z;n,t) = \begin{pmatrix} m_1 & m_2\end{pmatrix}, \text{ with } m_1\cdot m_2 = 1 \text{ and } m_1>0\,. \tag{11}$$

Here the phase θ of the jump matrix J is given by:

$$\theta(z;n,t) = t\left(z-z^{-1}\right) + 2n\log(z), \tag{12}$$

and it can be shown that $\overline{R(z)} = R(z^{-1})$ [30]. Furthermore, when $(a^0-1/2,b^0)$ decay exponentially, $R(z)$ is analytic in a neighborhood of $\mathbb{T}$. We only treat data that gives rise to an analytic reflection coefficient. The

solution $(a(t), b(t)) \in \ell(\mathbb{Z}) \times \ell(\mathbb{Z})$ to the initial value problem (1) for the Toda lattice can be recovered from the asymptotic behavior of m near $z = 0$:

$$m(z; n, t) = \begin{pmatrix} A_n(t)\big(1 - 2B_{n-1}(t)z\big) & \frac{1}{A_n(t)}\big(1 + 2B_n(t)z\big) \end{pmatrix} + \mathcal{O}\left(z^2\right), \tag{13}$$

where A and B are defined by

$$A_n(t) = \prod_{j=n}^{\infty} 2a_n(t) \quad \text{and} \quad B_n(t) = -\sum_{j=n+1}^{\infty} b_j(t)\,. \tag{14}$$

Remark 2.1. This meromorphic problem can be turned into an analytic problem by introducing small circles centered at each pole and using the appropriate jump conditions on these new contours [7]. Fix $\varepsilon > 0$ such that

$$\varepsilon < \frac{1}{2}\min\left\{\min_j\{|\zeta_j|\}, \min_j\{||\zeta_j| - 1|\}, \min_{j\neq l}\{|\zeta_j - \zeta_l|\}\right\}.$$

This choice of ε guarantees that the disks enclosed by the circles $D_j^{\pm} = \left\{z\colon \left|z - \zeta_j^{\pm 1}\right| = \varepsilon\right\}$, $j = 1, 2, \ldots, N$, do not intersect each other or the unit circle, and none of them contains the origin. We define $\widehat{m}$ by

$$\widehat{m}(z; n, t) = \begin{cases} m(z; n, t) \begin{pmatrix} 1 & 0 \\ \frac{\zeta_j \gamma_j e^{\theta(\zeta_j; n, t)}}{z - \zeta_j} & 1 \end{pmatrix}, & |z - \zeta_j| < \varepsilon, \;\; j = 1, 2, \ldots, N, \\ m(z; n, t) \begin{pmatrix} 1 & \frac{z\gamma_j e^{\theta(\zeta_j; n, t)}}{z - \zeta_j^{-1}} \\ 1 & 0 \end{pmatrix}, & |z - \zeta_j^{-1}| < \varepsilon, \;\; j = 1, 2, \ldots, N, \\ m(z; n, t), & \text{otherwise.} \end{cases} \tag{15}$$

It is straightforward to show that $\widehat{m}$ solves the following RH problem:

$$\widehat{m}^+(z; n, t) = \begin{cases} \widehat{m}^-(z; n, t) J(z; n, t), & z \in \mathbb{T}, \\ \widehat{m}^-(z; n, t) \begin{pmatrix} 1 & 0 \\ \frac{\zeta_j \gamma_j e^{\theta(\zeta_j; n, t)}}{z - \zeta_j} & 1 \end{pmatrix}, & z \in D_j^+, \;\; j = 1, 2, \ldots, N, \\ \widehat{m}^-(z; n, t) \begin{pmatrix} 1 & \frac{z\gamma_j e^{\theta(\zeta_j; n, t)}}{z - \zeta_j^{-1}} \\ 1 & 0 \end{pmatrix}, & z \in D_j^-, \;\; j = 1, 2, \ldots, N, \end{cases} \tag{16}$$

$$\widehat{m}(0; n, t) = \begin{pmatrix} m_1 & m_2 \end{pmatrix}, \text{ with } m_1 \cdot m_2 = 1 \text{ and } m_1 > 0,$$

where D_j^+ are oriented counter-clockwise and D_j^- are oriented clockwise.

Remark 2.2. The asymptotic condition (11) is not convenient for our numerical methods. As pointed out in [7], we can reduce our problem to a 2×2-matrix RH problem with the same jump and pole conditions but also with a standard condition at ∞, namely, normalization to the identity. More precisely, we consider the RH problem where we seek a function $\Phi\colon \mathbb{C} \setminus \mathbb{T} \to \mathbb{C}^{2\times 2}$ that is meromorphic, continuous up to $\mathbb{T}$, with simple poles at $\zeta_j^{\pm 1}$, $j = 1 \ldots, N$, and satisfies:

- *the jump condition:*

$$\Phi^+(z; n, t) = \Phi^-(z; n, t) J(z; n, t), \quad z \in \mathbb{T}, \quad J(z; n, t) = \begin{pmatrix} 1 - |R(z)|^2 & -\overline{R(z)} e^{-\theta(z; n, t)} \\ R(z) e^{\theta(z; n, t)} & 1 \end{pmatrix}, \tag{17}$$

- *the residue conditions:*

$$\begin{aligned} \operatorname*{Res}_{z=\zeta_j} \Phi(z; n, t) &= \lim_{z \to \zeta_j} \Phi(z; n, t) \begin{pmatrix} 0 & 0 \\ -\zeta_j \gamma_j e^{\theta(\zeta_j; n, t)} & 0 \end{pmatrix}, \quad j = 1, 2, \ldots, N, \\ \operatorname*{Res}_{z=\zeta_j^{-1}} \Phi(z; n, t) &= \lim_{z \to \zeta_j^{-1}} \Phi(z; n, t) \begin{pmatrix} 0 & \zeta_j^{-1} \gamma_j e^{\theta(\zeta_j; n, t)} \\ 0 & 0 \end{pmatrix}, \quad j = 1, 2, \ldots, N, \end{aligned} \tag{18}$$

- *the normalization condition:*

$$\Phi(\infty; n, t) = \lim_{z \to \infty} \Phi(z; n, t) = I\,. \tag{19}$$

The crucial observation here is that one can recover $m(0;n,t)$ from $\Phi^1(n,t) := \lim_{z\to\infty} z(\Phi(z;n,t)-I)$ and $\Phi(0;n,t)$ whenever the RH problem for Φ is uniquely solvable and reconstruct $(a_n(t), b_n(t))$ using (13). The solution procedure is summarized here:

(1) Assuming unique solvability for both Φ and m, compute $\Phi^1(n,t)$ and $\Phi(0;n,t)$ by solving the associated Riemann–Hilbert problem normalized to the identity at infinity.
(2) It should be the case that $m(z;n,t) = V^T\Phi(z;n,t)$ for some vector V. Enforce the symmetry condition (10)

$$V^T\Phi(0;n,t) = V^T\Phi(\infty;n,t)\begin{pmatrix}0 & 1\\ 1 & 0\end{pmatrix} = V^T\begin{pmatrix}0 & 1\\ 1 & 0\end{pmatrix}.$$

Then V must be in the nullspace of $\tilde{\Phi}(n,t) := \Phi(0;n,t) - \begin{pmatrix}0 & 1\\ 1 & 0\end{pmatrix}$ and the vector V can be fixed via the condition $m_1 \cdot m_2 = 1$.

By standard theory, $\det\Phi(z;n,t) = 1$ so that Φ has linearly independent rows. Thus, by the uniqueness of m, if $\tilde{\Phi}(n,t)$ is singular, it must have a one-dimensional nullspace. To see that $\tilde{\Phi}$ must be singular, consider the function

$$Y(z;n,t) = \begin{pmatrix}\Phi_{11}(z;n,t) & \Phi_{12}(z;n,t)\\ m_1(z;n,t) & m_2(z;n,t)\end{pmatrix}$$

where subscripts refer to components. Because neither m_1 nor m_2 can vanish at infinity, we can set $Z(z;n,t) = Y^{-1}(\infty;n,t)Y(z;n,t)$ so that $Z(\infty;n,t) = I$ and by uniqueness $\Phi = Z$. Therefore it suffices to take $V^T = \begin{pmatrix}0 & 1\end{pmatrix}Y(\infty;n,t)$ and V must exist and be unique.
(3) Once V is determined, we have

$$m(z;n,t) = V^T\Phi(z;n,t) = V^T(I+\Phi^1(n,t)z)\begin{pmatrix}0 & 1\\ 1 & 0\end{pmatrix} + \mathcal{O}(z^2), \quad z\to 0. \tag{20}$$

Remark 2.3. It is not *a priori* clear that a matrix solution of the meromorphic RH problem above exists. However, it can be inferred from the results of [7] that for any $n\in\mathbb{Z}$, a matrix solution of the above RH problem exists for $t \geq t^*(n)$, for some $0 < t^*(n) < \infty$. Furthermore, in practice, we never encounter values of (n,t) where solutions $\Phi(z;n,t)$ fail to exist.

We close this section with some final remarks on RH problems from [38] and [39]. Given an oriented contour Γ we define the Cauchy integral

$$\mathcal{C}_\Gamma u(z) = \frac{1}{2\pi i}\int_\Gamma \frac{u(s)}{s-z}\,ds.$$

It is well known that the operators defined by

$$\mathcal{C}_\Gamma^\pm = (\mathcal{C}_\Gamma u(z))^\pm$$

are bounded operators from $L^2(\Gamma)$ to itself. Moreover, these operators satisfy the identity

$$\mathcal{C}_\Gamma^+ - \mathcal{C}_\Gamma^- = I\,. \tag{21}$$

If we assume that the solution to an RH problem is of the form $\Phi = I + C_\Gamma u$, we can substitute this into the jump condition $\Phi^+ = \Phi^- J$ and use this identity to obtain

$$u - \mathcal{C}_\Gamma^- u\cdot(J-I) = J - I\,. \tag{22}$$

This is a singular integral equation (SIE) for u. We use $\mathcal{C}[J;\Gamma]$ to denote the operator in (22). This motivates the following definition.

Definition 2.4. A RH problem $[J;\Gamma]$ is said to be well-posed if $\mathcal{C}[J;I]$ is invertible with a bounded inverse on $L^2(\Gamma)$ and $J - I \in L^2(\Gamma)$.

This singular integral equation is critical in both the numerical and asymptotic solution of RH problems. A reader looking for a more in-depth discussion of RH problems should look to [2] for an introduction and [5, 6, 41] for a more advanced discussion. For numerical solution of RH problems, we refer the reader to [27, 36, 38]. A comprehensive discussion of the inverse scattering transform can be found in [1, 3].

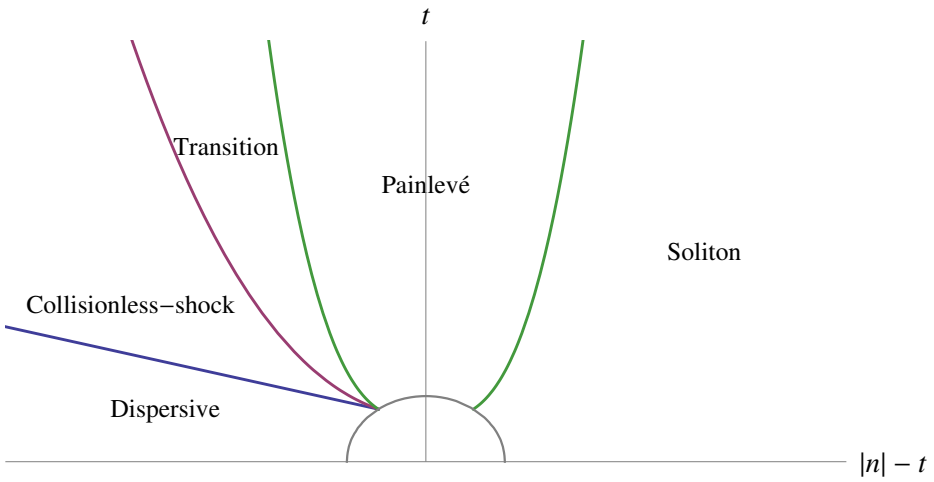

FIGURE 2. Asymptotic regions.

2.4. **Asymptotic regions.** In this section we discuss asymptotic regions for the long-time asymptotics of the Toda lattice with decaying initial data. A rigorous study of long-time asymptotics for solutions of the Toda lattice equations was recently carried out in [17] and [18] in the soliton and the dispersive regions (see below), but the question of long-time asymptotics in the region $|n|/t \sim 1$ has not been addressed in generality so far. Long-time behavior of solutions in this region was studied in [16] under the additional assumptions that no solitons are present, that is, the RH problem has no poles, and that $|R(z = \pm 1)| < 1$. Under the latter assumption, the solution is given asymptotically in terms of Painlevé II transcendents in the region $|n|/t \sim 1$, [16]. However, one generically has $R(z = \pm 1) = -1$. In this case, an additional region called the collisionless shock region appears as the stationary phase points of the jump matrix coalesce at $z = \pm 1$, and one needs to introduce additional contour deformations through employing the so-called g-function method, to bridge the dispersive and the Painlevé regions. In the current work, we present new deformations of the associated RH problem for the yet unstudied region $|n|/t \sim 1$ for generic initial data. We use these deformations for numerical purposes but fully believe they will be necessary for the rigorous asymptotic theory.

We introduce constants, $c_j > 0$, to divide asymptotic regions. While any valid choice of these will work, the numerical method can be improved by adjusting these on a case-by-case basis.

1. *The Dispersive region.* This region is defined for $|n| \leq c_1 t$, with $0 < c_1 < 1$. Asymptotics in this region were obtained in [18].
2. *The Collisionless shock region.* This region, to the best of our knowledge, has not been addressed in the literature. It is defined by the relation $c_1 t \leq |n| \leq t - c_2 t^{1/3} (\log t)^{2/3}$. Asymptotics are not known in this region.
3. *Transition region.* This region, to the best of our knowledge, is also not present in the literature. It is defined by the relation $t - c_2 t^{1/3} (\log t)^{2/3} \leq |n| \leq t - c_3 t^{1/3}$. Asymptotics are not known in this region. An analogue of this region was first introduced for KdV in [38].
4. *The Painlevé region.* This region is defined for $t - c_3 t^{1/3} \leq |n| \leq t + c_3 t^{1/3}$. Asymptotics in this region were obtained in [16] in absence of solitons and under the additional assumption that $|R(z)| < 1$.
5. *The Soliton region.* This region is defined for $|n| > t + c_3 t^{1/3}$. Let $v_k > 1$ denote the velocity of the k^{th} soliton and choose $\nu > 0$ so that the intervals $(v_k - \nu, v_k + \nu)$, $k = 1, 2, \ldots, N$, are disjoint. If $|n/t - v_k| < \nu$, the asymptotics in this region were obtained in [17] and [18].

2.5. **The numerical solution of Riemann–Hilbert problems.** Consider the contour $\Gamma = \bigcup_{j=1}^{n} \Gamma_j$ where each Γ_j is a non-self-intersecting smooth arc. Now, we restrict to considering contours where a sequence of Möbius transformations $M_1, \ldots, M_n$ are known such that $M_k([-1, 1]) = \Gamma_k$. Let $\mathbb{P}_m = \{\cos(j\pi/m) : j = 0, 1, \ldots, m\}$ be the Chebyshev points and let $T_m(x)$ denote the m^{th} Chebyshev polynomial of the first kind.

Given an RH problem

$$\Phi^+(z) = \Phi^-(z) J(z), \ z \in \Gamma, \ \Phi(\infty) = I, \tag{23}$$

which has smooth boundary values, the framework of Olver [21] (see also [36]) will typically return a vector V_j of function values at the mapped points $M_j(\mathbb{P}_{n_j})$, so that the function $U : \Gamma \to \mathbb{C}^{i\times j}$ defined piecewise by

$$U(z)|_{\Gamma_j} = \sum_{i=0}^{n_j} \alpha_i T_i(M_j^{-1}(z)),$$
$$U(M(\mathbb{P}_{n_j})) = V_j,$$

satisfies

- $I + \mathcal{C}_\Gamma U$ is a bounded function in $\mathbb{C} \setminus \Gamma$, and
- $I + \mathcal{C}_\Gamma U$ satisfies the RH problem (23) exactly at $M_j(\mathbb{P}_{n_j})$.

The points $\bigcup_j M_j(\mathbb{P}_{n_j})$ are called the collocation points.

We describe the method in more detail. Similar to before, substituting

$$\Phi \approx I + \mathcal{C}_\Gamma U \tag{24}$$

into the RH problem and using (21) gives a linear equation for U:

$$U - \mathcal{C}_\Gamma^- U \cdot (J - I) = J - I. \tag{25}$$

A closed-form expression for the Cauchy transform of the basis $T_i\big(M_j^{-1}(k)\big)$ [40] (see also [23]) allows the discretization of this linear equation by evaluating the Cauchy transform of the basis at the points $M_j(\mathbb{P}_{n_j})$. However, a modified definition for the Cauchy transform is required at the self-intersection (or junction) points points Γ_0 (which are included in the collocation points $M_j\big(\mathbb{P}_{n_j}\big)$), at which the Cauchy transform of this basis is unbounded. By assuming that the computed U is in the class of functions for which $I + \mathcal{C}_\Gamma U$ is bounded, we can define the bounded contribution of the Cauchy transform of each basis element at the points Γ_0. It can be shown, with appropriate assumptions on G (see the *product condition*, [33, Definition 3.8.3]) that the numerically calculated U must be in this class of functions. Therefore $I + \mathcal{C}_\Gamma U$ will be bounded and satisfies the RH problem at Γ_0, hence at all points in $M_j(\mathbb{P}_{n_j})$.

We use (24) to show that if $U \in L^1(\Gamma)$ then

$$\lim_{z\to\infty} z(\Phi(z) - I) = -\frac{1}{2\pi i}\int_\Gamma U(t)dt,$$

by the Dominated Convergence Theorem provided z is bounded away from Γ. The integral on the right-hand side can be computed using Clenshaw–Curtis quadrature. This relationship is needed in what follows to reconstruct the solution to the Toda lattice from the RH problem. The framework in [21, 23] gives an efficient method for computing $\mathcal{C}_\Gamma$ off Γ as well whenever Γ is the Möbius transformation of the unit interval.

Another aspect of the numerical solution of RH problems is contour truncation. Note that if $J(z^*) = I$ then the linear system (25) at this point becomes $U(z^*) = 0$. From this one can rigorously justify the removal of contours from the RH problem on which $\|J - I\|_{L^1\cap L^\infty}$ is small at the cost of a small error. This is discussed in more detail in [36, Chapter 2] and see [37] for a discussion of implementing this idea.

Remark 2.5. From the results in [21] it follows that spectral convergence (*i.e.* convergence that is faster than n^{-k} for any k where n is the number of collocation points) can be verified *a posteriori* for a well-posed RH problem by checking that the norm of the inverse of the discretization of $\mathcal{C}[J;\Gamma]$ grows at most algebraically. In the computations for this paper, we noticed at most logarithmic growth of the condition number for this collocation matrix, with a maximum on the order of 10^3.

3. Numerical computation of the scattering data

- Computing R.
  For $z \in \mathbb{T}$ we look for solutions of $L\varphi = \frac{1}{2}\left(z + z^{-2}\right)\varphi$ which behave like $z^{\pm n}$ as $n \to \pm\infty$. We define two new functions $f_+(z;n) = \varphi_+(z;n)z^{-n}$ and $f_-(z;n) = \varphi_-(z;n)z^n$ so that we have $f_\pm(z;n) \to 1$ as $n \to \pm\infty$. Then $f_\pm$ satisfies
  $$a_{n-1}z^{\mp 1}f_\pm(z;n-1) + \left(b_n - \tfrac{1}{2}\left(z + z^{-1}\right)\right)f_\pm(z;n) + a_n z^{\pm 1}f_\pm(z;n+1) = 0.$$
  This can be effectively solved using back substitution on $n \geq 0$ using the appropriate boundary conditions for $f_+(z;\cdot)$: for K large approximate f_+ by using the condition $f_+(z;K+1) = f_+(z;K) = 1$. The constant K is chosen so that $|b_m|$, $|a_m - 1/2|$ are both less than machine accuracy for $|m| \geq K$.

For $n \leq 0$ a similar method works for $f_-(z;\cdot)$ by setting $f_-(z;-K-1) = f_+(z;-K) = 1$. Matching these approximate solutions at $n = 0$ yields an approximation of the reflection coefficient.

- Computing $\{\zeta_1^{\pm 1}, \zeta_2^{\pm 1}, \ldots, \zeta_N^{\pm 1}\}$.
  Computing $\zeta_j^{\pm 1}$ is equivalent to computing the $\ell^2(\mathbb{Z})$ eigenvalues of the doubly-infinite Jacobi matrix L that is defined in (3). Noting that the set of limit points of $\bigcup_{K=1}^{\infty} \sigma(L_K)$, where L_K is a $K \times K$ truncation of L, is equal to the spectrum of L [4]. We approximate the eigenvalues of L by computing eigenvalues of a L_K that are outside the interval $[-1, 1]$ for a large value of K. This method might fail to capture eigenvalues of L that are close to its continuous spectrum. We present an example illustrating this case and provide the underlying spectral theory for Jacobi matrices in Appendix B. We check whether we successfully capture all of the eigenvalues by computing the inverse scattering transform at $t = 0$ and comparing the reconstructed solution to the initial data. If these values do not match, we employ Newton iteration to compute the (simple) zeros of $1/R(z)$, since, as mentioned in Section 2.2, $\zeta_j^{\pm 1}$ are the (simple) poles of the transmission coefficient, $T(z)$.
- Computing $\{\gamma_1, \gamma_2, \ldots, \gamma_N\}$.
  At the points $z = \zeta_j$, the solutions $\varphi_\pm(z;\cdot)$ are constant multiples of each other – and thus both lie in $\ell^2(\mathbb{Z})$ with exponential decay as $n \to \pm\infty$. We compute the norming constants by directly using their definition:

$$\gamma_j^{-1} = \|\varphi_+(\zeta_j;\cdot)\|^2_{\ell^2(\mathbb{Z})}\,. \tag{26}$$

4. Numerical solution of the inverse problem

In this section we present the required deformations of the RH problem for Φ. Every deformation involves explicit functions. Thus, once the RH problem is deformed and solved numerically, as discussed in Section 2.5, the original function Φ can be determined from the solution of the deformed problem. Another important fact is that if

$$\Phi(z;n,t) = A_1(z;n,t)A_2(z;n,t), \quad A_i(z) = I + A_{i,1}(n,t)z^{-1} + \mathcal{O}(z^{-2}), \quad z \to \infty,$$

then

$$\Phi(z;n,t) = I + (A_{1,1(n,t)} + A_{2,1}(n,t))z^{-1} + \mathcal{O}(z^{-2}), \quad z \to \infty. \tag{27}$$

In what follows, we often suppress n and t dependence for brevity in our notation and present the results and deformations for the case $n \geq 0$ and $t > 0$. It is straightforward to obtain the solution for the case $n < 0$ or $t > 0$ by modifying the initial data and using $n \geq 0$ [18]:

If $(a(t), b(t))$ solves the Toda lattice with initial data a_n^0 and b_n^0 and $(\tilde{a}(t), \tilde{b}(t))$ solves the Toda lattice with initial data a_{-n}^0 and $-b_{-n+1}^0$ then $a_{-n}(t) = \tilde{a}_n(t)$ and $b_{-n}(t) = -\tilde{b}_{n-1}(t)$.

To remove oscillations from the jump matrix, we examine the phase $\theta(z)$ that appears in these expressions. Solving $\theta'(z) = 0$ for z, the stationary phase points of θ are found to be

$$z_0^{\pm 1} = -\frac{n}{t} \pm \sqrt{\left(\frac{n}{t}\right)^2 - 1}\,.$$

Note that if $n = t$ or $n = -t$, the stationary phase points coalesce at $z = -1$, or $z = 1$, respectively.

Throughout our deformations we use the notation $\Phi_{\kappa,\alpha}$ for the solution of the deformed problem. The number κ indicates how many deformations have been performed, with $\kappa = 1$ being the original RH problem. The characters α are used to denote the region (*e.g.* $\alpha = \mathrm{cs}$ for the collisionless shock region.)

4.1. The Dispersive Region.

In this region, the stationary phase points $z_0^{\pm 1}$ of the exponent $\theta(z)$ lie on the unit circle, $\mathbb{T}$. We set $\Sigma = \{z\colon |z| = 1, |\operatorname{Re} z_0| < |\operatorname{Re} z|\}$ and $\Gamma = \mathbb{T} \setminus \Sigma$ as shown in Figure 3. Note that since $\operatorname{Re}\theta\left(z^{-1}\right) = -\operatorname{Re}\theta(z)$, the curves $\operatorname{Re}\theta(z) = 0$ are symmetric with respect to the mapping $z \mapsto z^{-1}$.

We now present the deformation from the initial RH problem. Assume we performed the deformation in Remark 2.1 to introduce small circles around each pole $\zeta_j^{\pm 1}$, $j = 1, 2, \ldots, N$, that is, we obtained $\widehat{\Phi}$ as instructed in (15). There are two cases to distinguish. If $\operatorname{Re}\theta(\zeta_j; n, t) < 0$ the jumps introduced in (16) have exponential decay to the identity as $t \to \infty$, which is what we desire. If $\operatorname{Re}\theta(\zeta_j; n, t)$, for some ζ_j, however, the jumps around such poles become unbounded for $t > 0$. Following the approach in [7] (see also [18]) we

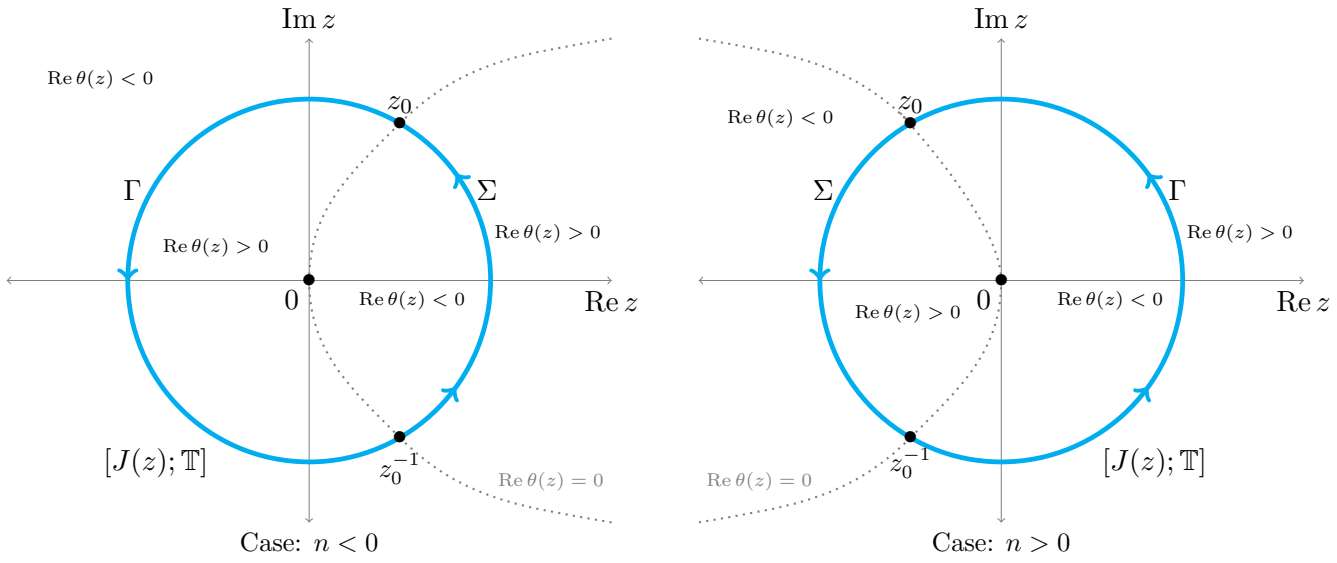

FIGURE 3. Sign of $\theta(z)$ and original contours for the RH problem in the dispersive region.

employ a conjugation procedure to restate our problem so that the contribution from these eigenvalues also becomes exponentially decaying to the identity as $t \to +\infty$. Let $K_{n,t} \subseteq \{1, 2, \dots, N\}$ denote the index set for ζ_j (if any) such that $|\gamma_j(t)| \exp\left(\operatorname{Re}\theta(\zeta_j; n, t)\right) > 1$. We set

$$Q(z) = \begin{pmatrix} \displaystyle\prod_{j \in K_{n,t}} \frac{z-\zeta_j}{z-\zeta_j^{-1}} & 0 \\ 0 & \displaystyle\prod_{j \in K_{n,t}} \frac{z-\zeta_j^{-1}}{z-\zeta_j} \end{pmatrix} \tag{28}$$

and for $j \in K_{n,t}$ define

$$\Phi_{1,\mathrm{d}}(z; n, t) = \begin{cases} \widehat{\Phi}(z; n, t) \begin{pmatrix} 1 & \frac{z-\zeta_j}{\gamma_j \zeta_j e^{\theta(\zeta_j; n, t)}} \\ -\frac{\zeta_j \gamma_j e^{\theta(\zeta_j; n, t)}}{z-\zeta_j} & 0 \end{pmatrix} Q(z), & |z - \zeta_j| < \varepsilon, \\ \widehat{\Phi}(z; n, t) \begin{pmatrix} 0 & \frac{z\zeta_j \gamma_j e^{\theta(\zeta_j; n, t)}}{z\zeta_j - 1} \\ -\frac{z\zeta_j - 1}{z\zeta_j \gamma_j e^{\theta(\zeta_j; n, t)}} & 1 \end{pmatrix} Q(z), & \left|z - \zeta_j^{-1}\right| < \varepsilon, \\ \widehat{\Phi}(z; n, t) Q(z), & \text{otherwise.} \end{cases} \tag{29}$$

Note that the matrices

$$\begin{pmatrix} 1 & \frac{z-\zeta_j}{\gamma_j \zeta_j e^{\theta(\zeta_j; n, t)}} \\ -\frac{\zeta_j \gamma_j e^{\theta(\zeta_j; n, t)}}{z-\zeta_j} & 0 \end{pmatrix} Q(z) \quad \text{and} \quad \begin{pmatrix} 0 & \frac{z\zeta_j \gamma_j e^{\theta(\zeta_j; n, t)}}{z\zeta_j - 1} \\ -\frac{z\zeta_j - 1}{z\zeta_j \gamma_j e^{\theta(\zeta_j; n, t)}} & 1 \end{pmatrix} Q(z)$$

have removable singularities at ζ_j and ζ_j^{-1}, respectively, and that $\lim_{z \to \infty} \Phi_{1,\mathrm{d}}(z; n, t) = I$ still holds. Recall that $D_j^{\pm} = \left\{ z \in \mathbb{C} \colon \left| z - \zeta_j^{\pm} \right| = \varepsilon \right\}$, where ε is chosen small enough so that $D_j^{\pm}$ do not intersect each other or any other contour. $\Phi_{1,\mathrm{d}}$ satisfies:

$$\Phi_{1,\mathrm{d}}^{+}(z; n, t) = \begin{cases} \Phi_{1,\mathrm{d}}^{-}(z; n, t) Q^{-1}(z) J(z; n, t) Q(z), & z \in \mathbb{T}, \\ \Phi_{1,\mathrm{d}}^{-}(z; n, t) Q^{-1}(z) \begin{pmatrix} 1 & \frac{z-\zeta_j}{\zeta_j \gamma_j e^{\theta(\zeta_j; n, t)}} \\ 0 & 1 \end{pmatrix} Q(z), & z \in D_j^{+}, \quad j \in K_{n,t} \\ \Phi_{1,\mathrm{d}}^{-}(z; n, t) Q^{-1}(z) \begin{pmatrix} 1 & 0 \\ \frac{z\zeta_j \gamma_j e^{\theta(\zeta_j; n, t)}}{z\zeta_j - 1} & 1 \end{pmatrix} Q(z), & z \in D_j^{-}, \quad j \in K_{n,t}, \end{cases} \tag{30}$$

$$\Phi(\infty; n, t) = I.$$

This successfully turns the exponential growth in the jump matrices into exponential decay to the identity. To simplify the notation, let $X_{j,\pm}$ denote the jump matrices that are used to invert the exponentials:

$$X_{j,+}(z;n,t) = \begin{pmatrix} 1 & \frac{z-\zeta_j}{\zeta_j\gamma_j e^{\theta(\zeta_j;n,t)}} \\ 0 & 1 \end{pmatrix} \quad \text{and} \quad X_{j,-}(z;n,t) = \begin{pmatrix} 1 & 0 \\ \frac{z\zeta_j-1}{z\zeta_j\gamma_j e^{\theta(\zeta_j;n,t)}} & 1 \end{pmatrix}, \tag{31}$$

and $Y_{j,\pm}(z;n,t)$ denote the jumps introduced in (16):

$$Y_{j,+}(z;n,t) = \begin{pmatrix} 1 & 0 \\ \frac{\zeta_j\gamma_j e^{\theta(\zeta_j;n,t)}}{z-\zeta_j} & 1 \end{pmatrix} \quad \text{and} \quad Y_{j,-}(z;n,t) = \begin{pmatrix} 1 & \frac{z\gamma_j e^{\theta(\zeta_j;n,t)}}{z-\zeta_j^{-1}} \\ 0 & 1 \end{pmatrix}. \tag{32}$$

We now present the deformation which will move the the oscillatory jumps along $\mathbb{T}$ into regions where the oscillatory terms decay exponentially. We define

$$\tau(z) = 1 - |R(z)|^2,$$

and note that the jump matrix $J(z;n,t)$ on $\mathbb{T}$ admits the following decompositions:

$$J(z;n,t) = M(z;n,t)P(z;n,t), \text{ with } M(z;n,t) = \begin{pmatrix} 1 & -R\left(z^{-1}\right)e^{-\theta(z;n,t)} \\ 0 & 1 \end{pmatrix}, P(z;n,t) = \begin{pmatrix} 1 & 0 \\ R(z)e^{\theta(z;n,t)} & 1 \end{pmatrix}$$

and

$$J(z;n,t) = L(z;n,t)D(z)U(z;n,t), \text{ with } L(z;n,t) = \begin{pmatrix} 1 & 0 \\ \frac{R(z)e^{\theta(z;n,t)}}{\tau(z)} & 1 \end{pmatrix}, U(z;n,t) = \begin{pmatrix} 1 & \frac{-R\left(z^{-1}\right)e^{-\theta(z;n,t)}}{\tau(z)} \\ 0 & 1 \end{pmatrix}$$

and

$$D(z) = \begin{pmatrix} \tau(z) & 0 \\ 0 & \frac{1}{\tau(z)} \end{pmatrix}.$$

We use the MP-decomposition on Γ, and the LDU-decomposition on Σ. M (for 'minus') will be deformed into the exterior ('minus' side) of the unit circle and P (for 'plus') will be deformed into the interior ('plus' side) of the unit circle. L is lower triangular and will be deformed into exterior of the unit circle. D is diagonal and will not be deformed[2]. U is upper triangular and will be deformed into interior of the unit circle. We employ these factorizations so that only one of $e^{\theta(z)}$ or $e^{-\theta(z)}$ appears in each matrix, which in turn makes it possible to obtain exponential decay in different regions of the complex plane. We introduce "ghost" contours, $\Sigma_\pm$, deformed into $\pm$ side of Σ, and $\Gamma_\pm$ deformed into $\pm$ side of Γ. Note that these new contours pass along the directions of steepest descent. We define a new matrix function $\Phi_{2,\mathrm{d}}$ based on the regions that emerge from this deformation, as shown in Figure 4(a). Note that the new definitions still satisfy the normalization condition at infinity. When $j \in K_{n,t}$ we use the jumps $X_{j,\pm}$ on $D_j^\pm$, respectively, in order to turn exponential growth into exponential decay as $t \to +\infty$. We use the jumps $Y_{j,\pm}$ on $D_j^\pm$ otherwise.

More precisely, $\Phi_{2,\mathrm{d}}$ satisfies:

$$\Phi_{2,\mathrm{d}}^+(z;n,t) = \begin{cases} \Phi_{2,\mathrm{d}}^-(z;n,t)Q^{-1}(z)L(z;n,t)Q(z), & z \in \Sigma_- \\ \Phi_{2,\mathrm{d}}^-(z;n,t)Q^{-1}(z)D(z)Q(z), & z \in \Sigma \\ \Phi_{2,\mathrm{d}}^-(z;n,t)Q^{-1}(z)U(z;n,t)Q(z), & z \in \Sigma_+ \\ \Phi_{2,\mathrm{d}}^-(z;n,t)Q^{-1}(z)M(z;n,t)Q(z), & z \in \Gamma_- \\ \Phi_{2,\mathrm{d}}^-(z;n,t)Q^{-1}(z)P(z;n,t)Q(z), & z \in \Gamma_+ \\ \Phi_{2,\mathrm{d}}^-(z;n,t)Q^{-1}(z)X_{j,\pm}(z;n,t)Q(z), & z \in D_j^\pm,\ j \in K_{n,t} \\ \Phi_{2,\mathrm{d}}^-(z;n,t)Q^{-1}(z)Y_{j,\pm}(z;n,t)Q(z), & z \in D_j^\pm,\ j \notin K_{n,t} \end{cases} \tag{33}$$

$$\Phi_{2,\mathrm{d}}^+(\infty;n,t) = I,$$

as seen in Figure 4(b). Note that the definitions of $\Gamma_\pm$ and $\Sigma_\pm$ are given in the figure.

Since generically $R(\pm 1) = -1$, the matrix D has a singularity at $z = -1$ (at $z = 1$ in the case $n < 0$) and we need to remove this singularity in order to represent the solution by Chebyshev polynomials (see Section 2.5

[2]Note that as the amplitude of the initial data increases, $|R(z)|$ can approach unity. This can cause numerical issues as $D(z)$ is then ill-conditioned and some additional precondition steps may be required. This is not an issue for the examples we consider in this paper.

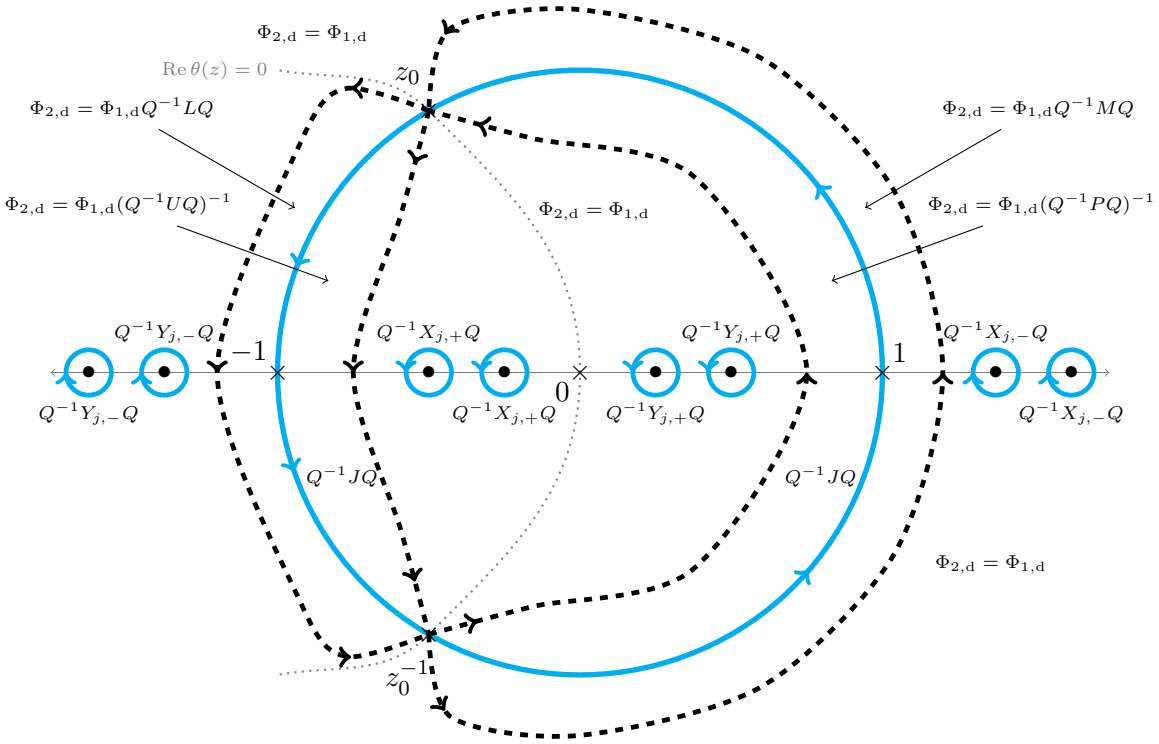

(a)

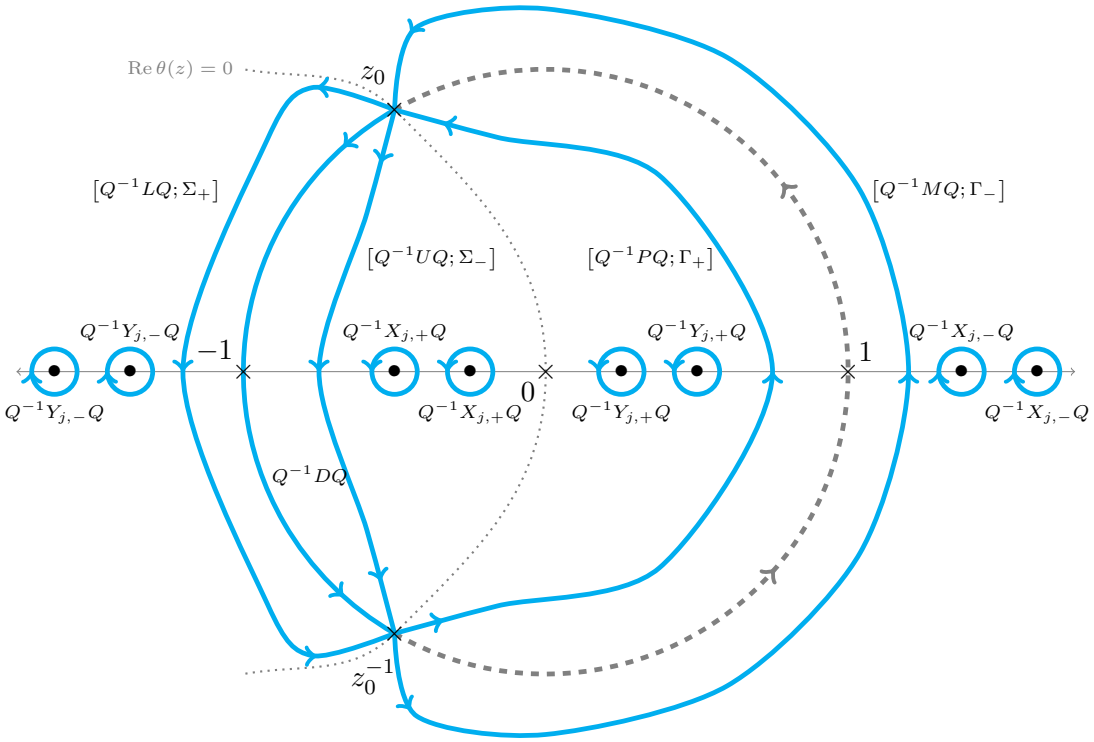

(b)

FIGURE 4. (a) Jump contours (blue) and matrices for the initial RH problem for with 'ghost' contours (dashed black), (b) Jump contours and matrices for the RH problem satisfied by $\Phi_{2,\mathrm{d}}$. This figure contains the definitions of $\Gamma_\pm$ and $\Sigma_\pm$.

for details on numerical solution of RH problems). We also need the jump matrix to approach the identity to achieve asymptotic stability. We must remove the jump on the contour Σ (see Figure 3). We introduce the unique 2×2 matrix-valued function Δ that solves the diagonal RH problem:

$$\Delta^+(z;n,t)=\Delta^-(z;n,t)D(z),\quad z\in\Sigma,\quad \Delta(\infty;n,t)=I, \tag{34}$$

such that Δ is bounded for z in a neighborhood of z_0,z_0^{-1}. The exact form of Δ can be found in the Appendix A. Note that in general Δ has singularities at the end points $z=z_0^{\pm 1}$ of the contour. To combat this issue we introduce circles around both $z_0^{\pm 1}$, see Figure 5.

We define $\Phi_{3,\mathrm{d}}$ as shown in Figure 5(b), where $\Phi_{3,\mathrm{d}}=\Phi_{2,\mathrm{d}}$ when no definition is specified; and we see that $\Phi_{3,\mathrm{d}}$ satisfies the RH problem that is presented in Figure 5(c). We apply the same procedure at z_0^{-1}. Finally we define $\Phi_{4,\mathrm{d}}=\Phi_{3,\mathrm{d}}\Delta^{-1}$ and see that $\Phi_{4,\mathrm{d}}$ satisfies the RH problem shown graphically in Figure 6. We solve this resulting RH problem numerically, use (27) to find $\Phi^1(n,t)$ and $\Phi(0;n,t)$ and use this to compute $A_n(t)$ and $B_n(t)$ (and hence $a_n(t)$ and $b_n(t)$) as discussed in (20).

We follow the methodology put forth in [38] to determine the radius of the circles near z_0 and z_0^{-1}. Near z_0 we have

$$\theta(z;n,t)=\theta(z_0;n,t)-2\frac{t+nz_0}{z_0^3}(z-z_0)^2+\mathcal{O}(z-z_0)^3.$$

We choose the radius of the circles to be proportional to $r(n,t)=\sqrt{\frac{|z_0|^3}{|t+nz_0|}}$ so that for $s=(z-z_0)/(cr(n,t))$, $|z-z_0|=|cr(n,t)|$

$$\tilde\theta(s;n,t):=\theta\left(z_0+scr(n,t);n,t\right))=\theta(z_0;n,t)-\tilde c s^2(1+o(1)), \tag{35}$$

where $\tilde c$ is proportional to c^2 and accounts for the phase. Because $\theta(z_0;n,t)$ is purely imaginary, $e^{\tilde\theta(s;n,t)}$ is bounded if s is bounded. It it also follows that for $|n|/t\le c_1$, in the dispersive region, that $r(n,t)=\mathcal{O}(t^{-1/2})$ so one may use $r(n,t)=ct^{-1/2}$, in practice.

4.2. **The Painlevé Region.** For $\frac{n}{t}>1$ this region intersects with the soliton region defined below, and we use that deformation. For $\frac{n}{t}<1$, the saddle points are coalescing at $z=-1$ and this allows for a new deformation. Consider the arc Σ that passes from $z=-1$ and the two stationary phase points $z_0^{\pm 1}$ as shown in Figure 3. Set $z=e^{i(\pi-\omega)}$ and $z_0=e^{i(\pi-\omega_0)}$ with $\cos(\pi-\omega_0)=-\frac{n}{t}$. Thus $z\in\Sigma$ if and only if $|\omega|<|\omega_0|$, and $\omega_0\to 0$ as $t\to\infty$. Choose the branch cut $(0,\infty)$ for the logarithm. Then $\theta(z;n,t)$ can be expressed in terms of ω as by abusing notation:

$$\theta(\omega;n,t)=2i\left(t\sin\omega+n(\pi-\omega)\right).$$

Note that $\frac{|n|}{t}\ge 1-ct^{-2/3}$ implies

$$|\sin(\pi-\omega)|\le\sin\omega_0\le\sqrt{2c}t^{-1/3}\sqrt{1-\tfrac{c}{2}t^{-2/3}}=\sqrt{2c}t^{-1/3}\left(1-\frac{c}{4}t^{-2/3}+\frac{c}{16}t^{-4/3}+\mathcal{O}\left(t^{-2}\right)\right).$$

for large values of t. This together with $t-|n|<ct^{1/3}$ yields

$$|\theta(\omega;n,t)-2\pi in|=|t\sin(\pi-\omega)-n\omega|\le|\sin\omega_0|\big(t-|n|\big)\le\sqrt{2}c^2+\mathcal{O}(t^{-2/3}),$$

for $|\omega|<\omega_0$, which implies that the oscillations are controlled between the two stationary points and the LDU factorization is not needed. See Figure 7 for the RH problem in this region.

4.3. **The Collisionless shock Region.** The singularity at $z=-1$ in the matrix $D(z)$ destroys the boundedness of the parametrix[3] $\Delta(z;n,t)$. As $z\to-1$, the matrices $\Delta Q^{-1}MQ\Delta^{-1}$ and $\Delta Q^{-1}PQ\Delta^{-1}$ are unbounded and we cannot bridge the dispersive region and the Painlevé region. By adjusting the constants that determine the asymptotic regions we can make the dispersive and Painlevé regions overlap up to some finite t, but we wish to obtain a method which is stable for large values of t. To achieve this stability, we need to introduce additional deformations. The analogous region for the KdV equation has been introduced in [28] and the deformations were derived in [8]. The asymptotic analysis of the solutions, the scaling, and the

[3]We use the term parametrix in a different way than is typical in the asymptotic analysis of RH problems. We use the term for any function that solves, or regularizes, any portion of the RH problem.

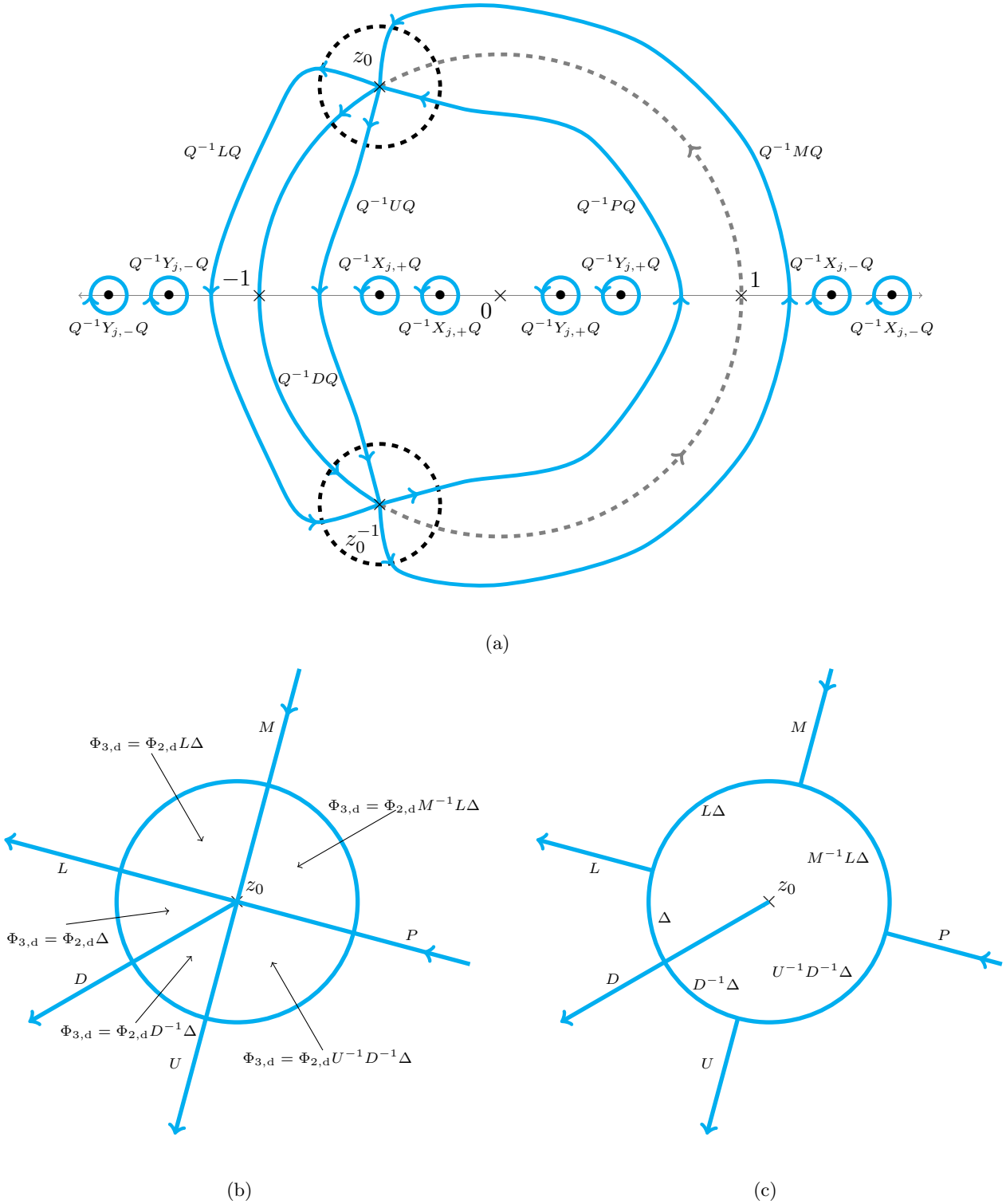

FIGURE 5. (a) 'Ghost' circles in preparation for the singularities of Δ, (b) Definitions of $\Phi_{3,\mathrm{d}}$ near z_0, (c) The jump contours and matrices of the RH problem satisfied by $\Phi_{3,\mathrm{d}}$ near z_0.

needed deformations for the Toda lattice in this region, to the best of our knowledge, are not present in the literature.

As n increases in the dispersive region, the stationary phase points of $e^{\theta(z)}$ approach the singularity ($z = -1$) of the parametrix Δ. We replace the phase θ by a so-called g-function as was done for KdV in [12] (see also [38]). In what follows, we define $g(z)$ as solution of an RH problem with the properties that are tailored to

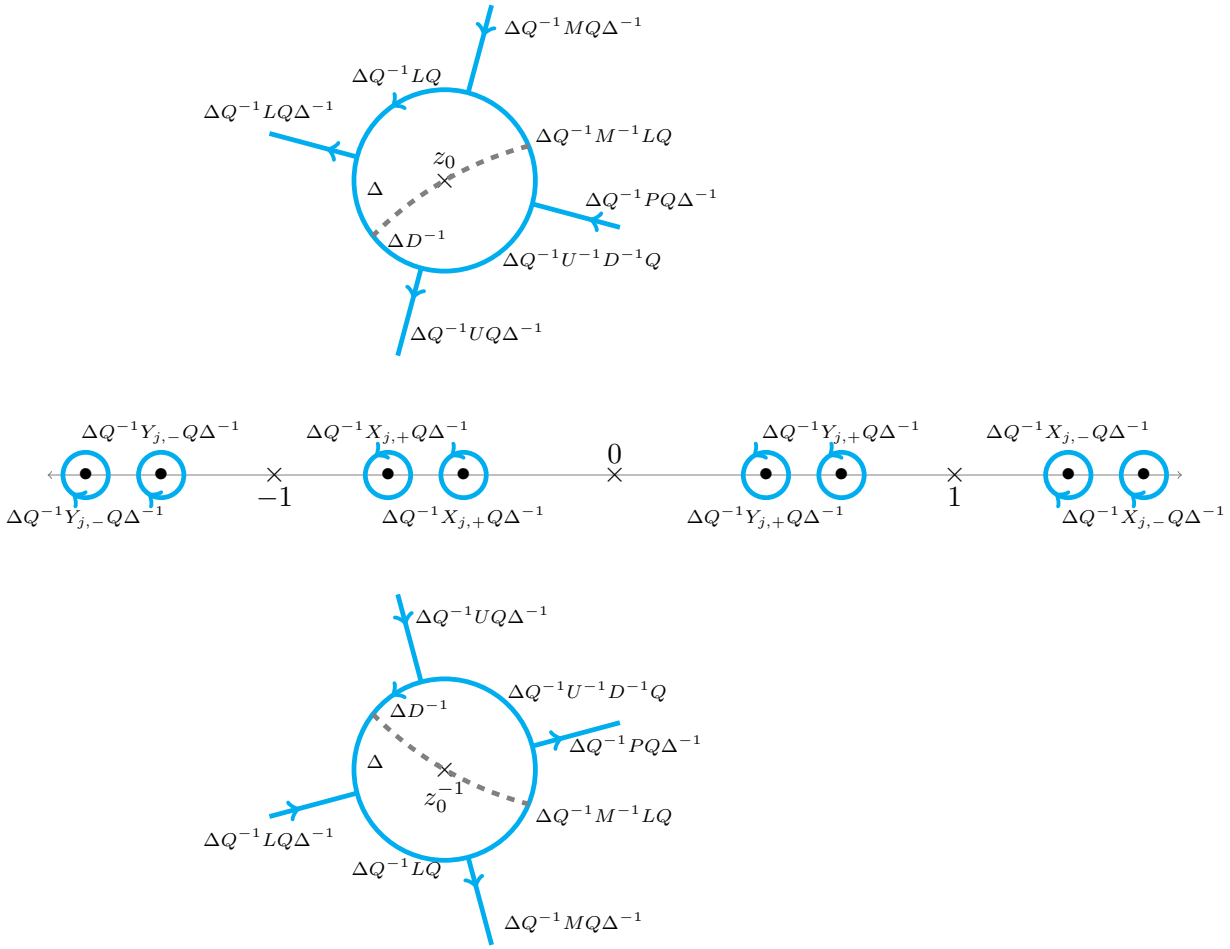

FIGURE 6. A zoomed view of the jump contours and matrices for the RH problem in the dispersive region.

achieve the task described above. Having done that, we introduce the needed deformations in this region. We leave the implementation details for solution of the RH problem given in (36) to Subsection C.3. In Appendix C.1, we explicitly construct the g-function.

From here on throughout the text, we let $\lambda_0 \in [-1, 0]$ and $\rho_0 \in [0, 1]$ denote the real and imaginary parts of the stationary phase point z_0, respectively. That is,

$$\lambda_0 = -\frac{n}{t} \quad \text{and} \quad \rho_0 = \sqrt{1 - \left(\frac{n}{t}\right)^2}.$$

For z_1, $z_2 \in \mathbb{T}$, $z_1 \neq z_2$ define

$$(z_1, z_2)_{\text{arc}} = \left\{ e^{i\theta} : \min\{\arg z_1 \mod 2\pi,\ \arg z_2 \mod 2\pi\} < \theta < \max\{\arg z_1 \mod 2\pi,\ \arg z_2 \mod 2\pi\} \right\}$$

oriented from z_1 to z_2. Then $[z_1, z_2]_{\text{arc}}$ is the closure of $(z_1, z_2)_{\text{arc}}$. For $\alpha, \beta \in \mathbb{T}$ with $-1 \leq \operatorname{Re}\alpha \leq \lambda_0 \leq 0 \leq \operatorname{Re}\beta \leq 1$, we label $\Sigma_u = [\beta, \alpha]_{\text{arc}}$, $\Sigma_c = \left[\alpha, \alpha^{-1}\right]_{\text{arc}}$, and $\Sigma_l = \left[\alpha^{-1}, \beta^{-1}\right]_{\text{arc}}$, as shown in Figure 8.

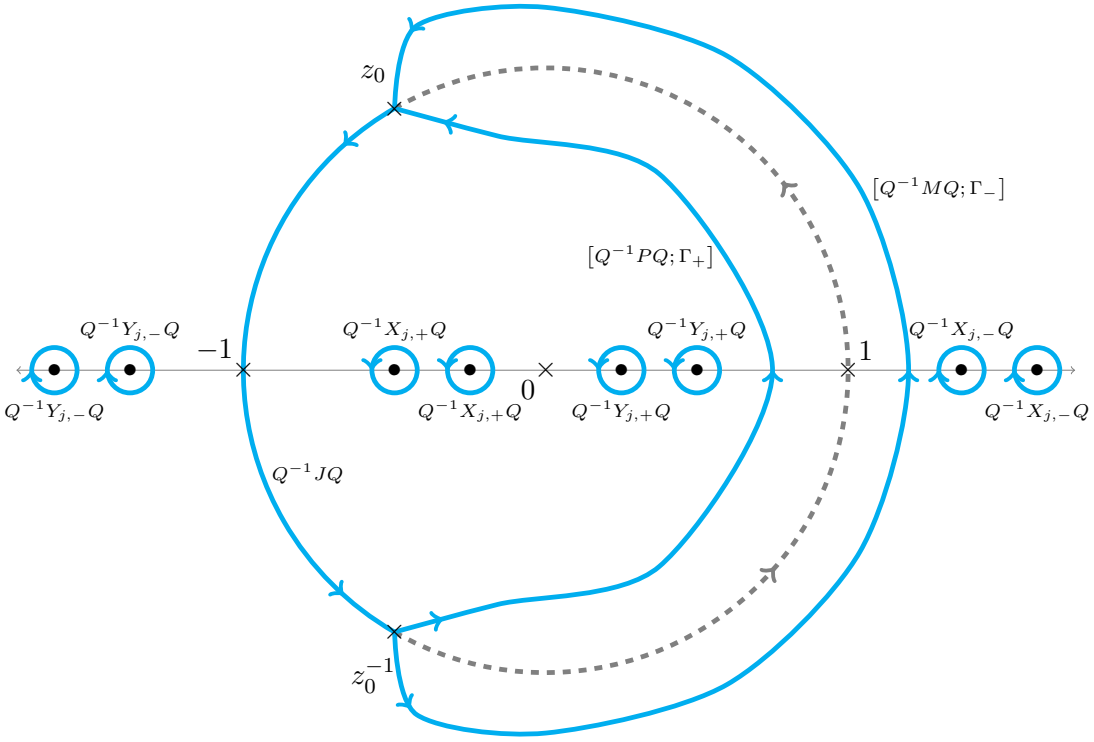

FIGURE 7. The jump contours and matrices for the RH problem in the Painlevé region with $0 < n < t$.

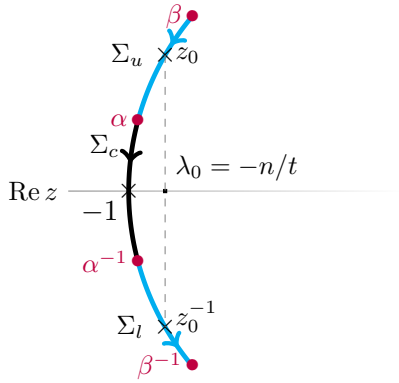

FIGURE 8. The cuts Σ_u, Σ_c, and Σ_l for $0 < n < t$.

Following the approach in [38], we determine α and β on the unit circle so that there exists a function $g(z)$ that satisfies the following properties:

$$
\begin{aligned}
&g^+(z) + g^-(z) = \begin{cases} d_1 & \text{if } z \in \Sigma_u, \\ -d_1 & \text{if } z \in \Sigma_l, \end{cases} \\
&g^+(z) - g^-(z) = d_2, \quad z \in \Sigma_c, \\
&g(z) - \frac{1}{2t}\theta(z) \text{ analytic in } z \text{ off } \left[\beta, \beta^{-1}\right]_{\text{arc}} = \Sigma_u \cup \Sigma_c \cup \Sigma_l, \\
&g(z) \text{ is bounded at } z = \alpha^{\pm 1} \text{ and } z = \beta^{\pm 1}, \\
&g(z) = \tfrac{1}{2}z - \lambda_0 \log z + \mathcal{O}\left(z^{-1}\right) \text{ as } z \to \infty,
\end{aligned}
\tag{36}
$$

for some complex constants d_1 and d_2. These constants depend on α and β. We leave the details of our method to solve this RH problem to Appendix C.3. Define the function $\mathfrak{g}(z) = t\left(g(z) - \frac{1}{2t}\theta(z)\right)$, and construct the

matrix

$$\phi(z) = \begin{pmatrix} e^{\mathfrak{g}(z)} & 0 \\ 0 & e^{-\mathfrak{g}(z)} \end{pmatrix} \to I \text{ as } z \to \infty.$$

Notice that, for $z \in \mathbb{T}$ the jump satisfied by $\Phi(z)\phi(z)$ is $\phi_-^{-1}J(z)\phi_+(z)$ in the absence of solitons. If solitons are present, we replace J by $Q^{-1}JQ$. Explicitly,

$$\phi_-^{-1}J(z)\phi_+(z) = \begin{pmatrix} \left[1 - R(z)R\left(z^{-1}\right)\right] e^{\mathfrak{g}^+(z)-\mathfrak{g}^-(z)} & -R\left(z^{-1}\right) e^{-\theta(z)-\mathfrak{g}^+(z)-\mathfrak{g}^-(z)} \\ R(z)e^{\theta(z)+\mathfrak{g}^+(z)+\mathfrak{g}^-(z)} & e^{-\mathfrak{g}^+(z)+\mathfrak{g}^-(z)} \end{pmatrix}. \tag{37}$$

Note that $\mathfrak{g}$ satisfies

$$\begin{aligned} \mathfrak{g}^+(z) - \mathfrak{g}^-(z) &= t\left(g^+(z) - g^-(z)\right) = 0, \text{ for } z \notin \left[\beta, \beta^{-1}\right]_{\text{arc}} \\ \mathfrak{g}^+(z) + \mathfrak{g}^-(z) &= t\left(g^+(z) + g^-(z)\right) - \theta(z) \to 0 \text{ as } z \to \infty. \end{aligned}$$

We have

$$\phi_-^{-1}(z)J(z)\phi^+(z) = \begin{cases} \begin{pmatrix} 1 - R(z)R\left(z^{-1}\right) & -R\left(z^{-1}\right) e^{-2tg(z)} \\ R(z)e^{2tg(z)} & 1 \end{pmatrix}, & z \in (1, \beta)_{\text{arc}}, \\ \begin{pmatrix} \left[1 - R(z)R\left(z^{-1}\right)\right] e^{t\left(g^+(z)-g^-(z)\right)} & -R\left(z^{-1}\right) e^{-\delta_1} \\ R(z)e^{\delta_1} & e^{t\left(-g^+(z)+g^-(z)\right)} \end{pmatrix}, & z \in (\beta, \alpha)_{\text{arc}}, \\ \begin{pmatrix} \left[1 - R(z)R\left(z^{-1}\right)\right] e^{\delta_2} & -R\left(z^{-1}\right) e^{-t\left(g^+(z)+g^-(z)\right)} \\ R(z)e^{t\left(g^+(z)+g^-(z)\right)} & e^{-\delta_2} \end{pmatrix}, & z \in \left(\alpha, \alpha^{-1}\right)_{\text{arc}}, \\ \begin{pmatrix} \left[1 - R(z)R\left(z^{-1}\right)\right] e^{t\left(g^+(z)-g^-(z)\right)} & -R\left(z^{-1}\right) e^{\delta_1} \\ R(z)e^{-\delta_1} & e^{t\left(-g^+(z)+g^-(z)\right)} \end{pmatrix}, & z \in \left(\alpha^{-1}, \beta^{-1}\right)_{\text{arc}}, \\ \begin{pmatrix} 1 - R(z)R\left(z^{-1}\right) & -R\left(z^{-1}\right) e^{-2tg(z)} \\ R(z)e^{2tg(z)} & 1 \end{pmatrix}, & z \in \left(\beta^{-1}, 1\right)_{\text{arc}}, \end{cases} \tag{38}$$

where $\delta_1/t = g^+(z) + g^-(z)$ for $z \in \Sigma_u$, and $\delta_2/t = g^+(z) - g^-(z)$ for $z \in \Sigma_c$, and $\theta(z)$ disappears from the problem. As in the dispersive region, we proceed with using the factorization $J = LDU$ on Σ_c. Again, D has a singularity at $z = -1 \in \Sigma_c$ that has to be removed. We analyze the jump matrix on Σ_c in the limit $z_0 \to -1$ to determine δ_1 and δ_2 (hence d_1 and d_2 in (36)). On $\Sigma_c = \left(\alpha, \alpha^{-1}\right)_{\text{arc}}$, the jump matrix is given by

$$\phi_-^{-1}(z)D(z)\phi_+(z) = \begin{pmatrix} \left[1 - R(z)R\left(z^{-1}\right)\right] e^{\delta_2} & 0 \\ 0 & \left(\left[1 - R(z)R\left(z^{-1}\right)\right] e^{\delta_2}\right)^{-1} \end{pmatrix}. \tag{39}$$

Using $R(-1) = -1$ and the analyticity of $R(z)$ in a neighborhood around $z = -1$, we observe that

$$1 - R(z)R\left(z^{-1}\right) = \nu(z+1)^2 + \mathcal{O}\left((z+1)^4\right) \text{ near } z = -1, \tag{40}$$

for some constant $\nu \in \mathbb{C}$. So far, we have left α and β mostly arbitrary. It follows that (see Appendix C.1) the prescribed asymptotic behavior for $g(z)$ requires $\operatorname{Re}\alpha + \operatorname{Re}\beta = 2\lambda_0$, leaving us with single degree of freedom. Now consider the affine transformation, $k = K(z)$, defined by

$$K(z) = i\left(\frac{z - \lambda_0}{\rho_0}\right), \quad z(k) = K^{-1}(k) = \lambda_0 - i\rho_0 k. \tag{41}$$

Note that this transformation fixes the stationary phase points: $K\left(z_0^{\pm 1}\right) = \mp 1$, and the image of the contour $\left(\beta, \beta^{-1}\right)_{\text{arc}}$ under the mapping K flattens as $z_0^{\pm 1} \to -1$ (see Figure 9). To remove the singularity at of $D(z)$ at $z = -1$, we need to obtain the parametrix $\psi(z)$ by solving the diagonal RH problem:

$$\psi^+(z) = \psi^-(z)\phi_-^{-1}(z)D(z)\phi_+(z), \ z \in \Sigma_c, \ \psi(\infty) = I, \tag{42}$$

which, in the new variables (41), reads

$$H^+(k) = H^-(k)\widetilde{D}(k), \ k \in K(\Sigma_c), \tag{43}$$

where $K^{-1}(k) = z(k)$, $H(k) = \psi\left(K^{-1}(k)\right)$, and $\widetilde{D}(k) = \phi_-^{-1}(K^{-1}(k))\, D(K^{-1}(k))\, \phi_+\left(K^{-1}(k)\right)$. Let $k^* = K(-1)$ so that $z(k) + 1 = -i\rho_0(k - k^*)$. We choose δ_2 to enforce $\rho_0^2 e^{\delta_2} = 1$ so that the $(1,1)$-entry of the diagonal jump matrix $\widetilde{D}(z)$ satisfies

$$\left[1 - R\left(z(k)\right) R\left(z(k)^{-1}\right)\right] e^{\delta_2} = \nu(k - k^*)^2 + \mathcal{O}\left(\rho_0^2 (k - k^*)^4\right), \quad \text{near} \quad z = -1,\ k = k^*, \tag{44}$$

hence removing, up to second order, the dependence on ρ_0. This indicates that $\widetilde{D}(z)$ remains bounded as $\rho_0 \to 0$ which ensures the boundedness of H, and hence of ψ as $t \to \infty$. In Appendix C.1 it is shown that α and β can (and should) be chosen so that

$$\frac{-\log \rho_0^2}{t} = \int_\beta^\alpha \frac{1}{p^2} \sqrt{(p-\alpha)\left(p-\alpha^{-1}\right)(p-\beta)\left(p-\beta^{-1}\right)}^{+}\, dp. \tag{45}$$

Loosely speaking, the collisionless shock region is defined to be the region in the (n,t)-plane where this is solvable for α and β and $\alpha + 1$ is not too small. This reasoning gives the asymptotic condition $n = t - c_2 t^{1/3} (\log t)^{2/3}$. See Appendix C.2 for more detail.

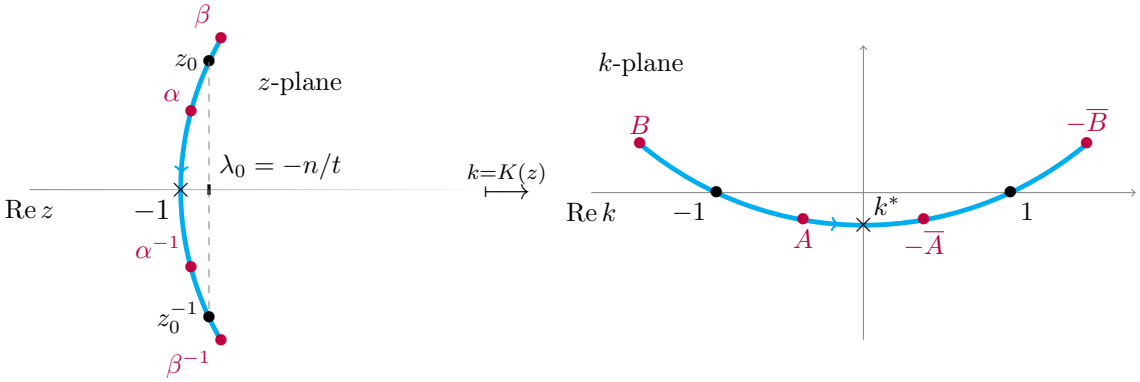

FIGURE 9. Cuts mapped under the affine mapping $z \mapsto K(z)$.

Thus, to obtain a local parametrix, we solve the diagonal RH problem (42) which can be solved explicitly, in the same way as the parametrix Δ in Section 4.1. The full deformation for this region now follows. We lens the problem into the form shown in Figure 10(a). The jumps and contours near α^{-1} and β^{-1} are given in Figure 10(b). What happens near α and β is clear by symmetry. We define $\Phi_{2,\mathrm{cs}}$ inside the circles centered at α and α^{-1} as shown in Figure 11(a) and leave $\Phi_{2,\mathrm{cs}} = \Phi_{1,\mathrm{cs}}$ everywhere else. The RH problem satisfied by $\Phi_{2,\mathrm{cs}}$ near the points α^{-1} and β^{-1} is shown in Figure 11(b).Define $\Phi_{3,\mathrm{cs}}$ by

$$\Phi_{3,\mathrm{cs}}(z) = \begin{cases} \Phi_{2,\mathrm{cs}}(z), & \text{inside the circles centered at } \alpha^{\pm 1} \text{ and } \beta^{\pm 1}, \\ \Phi_{2,\mathrm{cs}}(z)\phi(z), & \text{outside the circles centered at } \alpha^{\pm 1} \text{ and } \beta^{\pm 1}. \end{cases} \tag{46}$$

The RH problem satisfied by $\Phi_{3,\mathrm{cs}}$ near the points α^{-1} and β^{-1} is shown in Figure 12. Finally, once ψ is obtained, we conjugate the problem by ψ as was done with Δ in Section 4.1, and define $\Phi_{4,\mathrm{cs}}$ by

$$\Phi_{4,\mathrm{cs}}(z) = \begin{cases} \Phi_{3,\mathrm{cs}}(z)\psi^{-1}(z), & \text{outside the circles centered at } \alpha \text{ and } \alpha^{-1}, \\ \Phi_{3,\mathrm{cs}}(z), & \text{inside the circles centered at } \alpha \text{ and } \alpha^{-1}. \end{cases}$$

The final deformation for this region and the RH problem satisfied by $\Phi_{4,\mathrm{cs}}$ is shown in Figure 13. The radii of the circles round α, β, α^{-1} and β^{-1} must be specified. It is easily seen from (61) that $g'(z)$ vanishes as a square root at each of these points and $g(z) = a + b(z-c)^{3/2}$ for $c = \alpha$, β, α^{-1} or β^{-1} and a, b depend on the choice of c. Following the arguments in (35) we choose the radius of these circles to be proportional to $t^{-2/3}$, of course, under the constraint that the circles should not intersect one another.

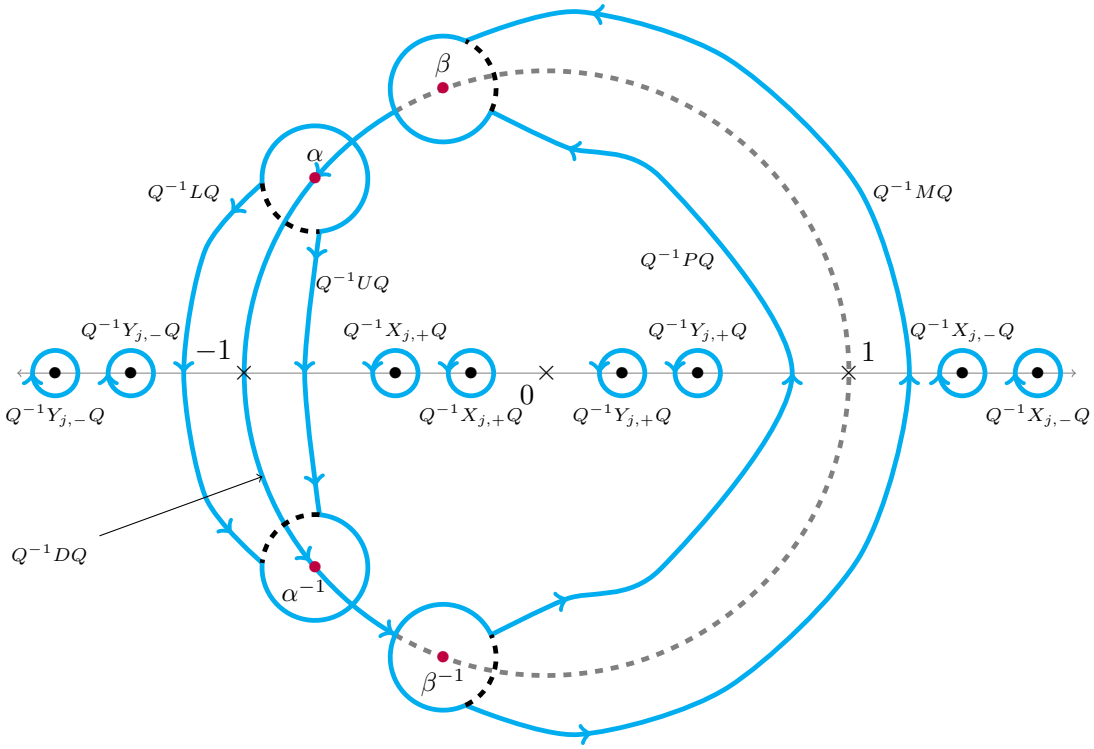

(a)

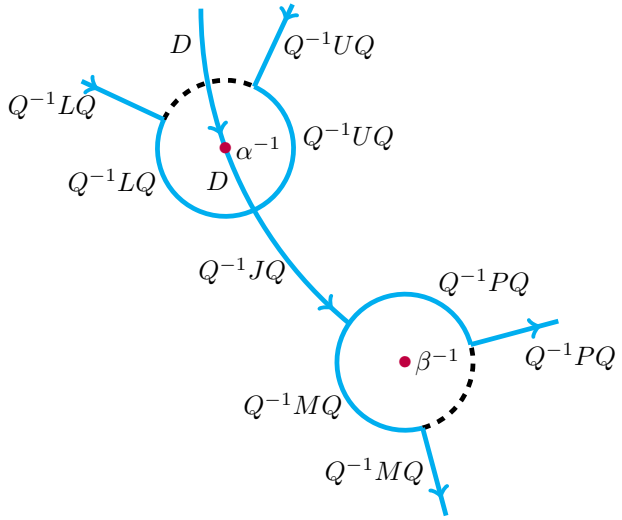

(b)

FIGURE 10. (a) The initial deformation of the RH problem in the collisionless shock region for a function $\Phi_{1,\mathrm{cs}}$, (b) The initial jump contours and matrices near α^{-1}, β^{-1}.

4.4. **The Transition Region.** Similar to the case for the KdV equation (see [38]), the deformations in the collisionless shock region extends the values of (n,t) for which there exists a well-behaved RH problem past that of the Dispersive region. However, this is not asymptotically reliable as we approach the Painlevé region: as $|n|-t$ decreases, α and α^{-1} (defined in the previous section) approach the singularity of the parametrix ψ (see (42)) at $z=-1$ (at $z=1$ for the case $n<0$). To avoid this issue, we collapse the lensing on

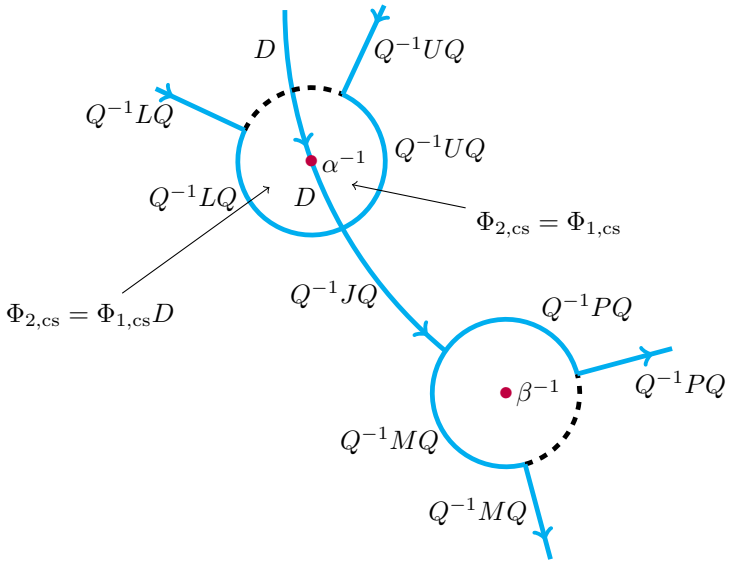

(a)

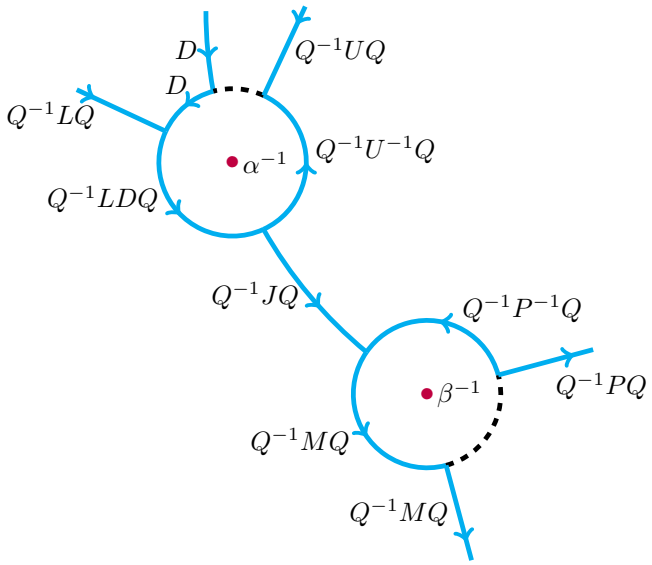

(b)

FIGURE 11. (a) Definition of $\Phi_{2,\mathrm{cs}}$ near α^{-1}, β^{-1}, (b) The jump contours and matrices for the RH problem for $\Phi_{2,\mathrm{cs}}$ near α^{-1}, β^{-1}.

$\Sigma_c = \left(\alpha, \alpha^{-1}\right)_{\mathrm{arc}}$ and in order to maintain numerical accuracy, we choose α to ensure that the oscillations are controlled on $\left[\beta, \beta^{-1}\right]_{\mathrm{arc}}$. Let $n = t - t^{1/3} r(t)$, where

$$\lim_{t\to\infty} \frac{r(t)}{(\log t)^{2/3}} = 0, \quad \text{and} \quad \lim_{t\to\infty} r(t) = \infty.$$

Given a positive bounded function $f(n,t)$ we choose α and β by enforcing (recall that $\operatorname{Re}\alpha + \operatorname{Re}\beta = 2\lambda_0$) [4]

$$\frac{f(n,t)}{t} = -i \int_{-1}^{\alpha} \frac{1}{p^2} \sqrt{(p-\alpha)\left(p-\alpha^{-1}\right)(p-\beta)\left(p-\beta^{-1}\right)}\, dp. \tag{47}$$

[4] In practice we use $f(n,t) = 2$. Other choices may result in more accurate computations.

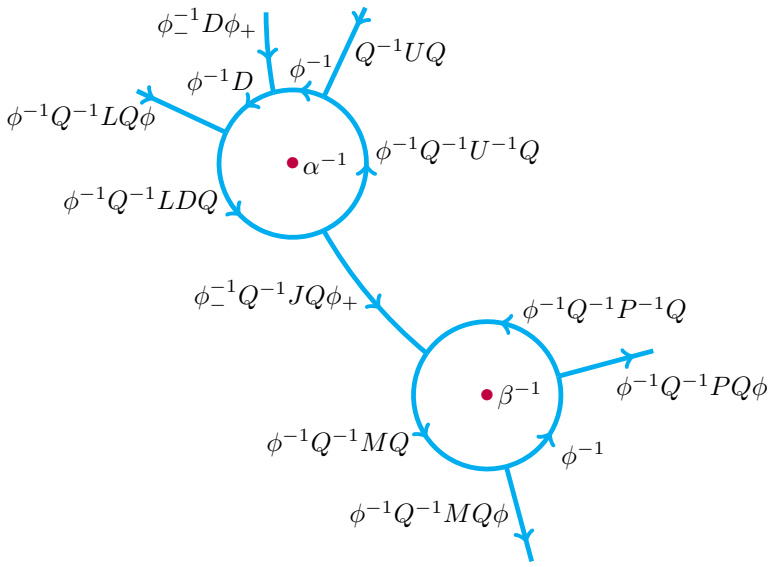

FIGURE 12. The jump contours and matrices for the RH problem for $\Phi_{3,\mathrm{cs}}$ near α^{-1}, β^{-1}.

In light of (63), this is equivalent to

$$\begin{aligned} t\big(g^+(z)+g^-(z)\big) &= if(n,t) \quad \text{for} \quad z\in(\beta,\alpha)_{\mathrm{arc}}\,,\\ t\big(g^+(z)+g^-(z)\big) &= -if(n,t) \quad \text{for} \quad z\in\big(\alpha^{-1},\beta^{-1}\big)_{\mathrm{arc}}\,. \end{aligned} \tag{48}$$

By adjusting f, (47) can be solved for α since the right hand side is a monotone function of α under the constraint $\operatorname{Re}\alpha+\operatorname{Re}\beta=2\operatorname{Re}\lambda_0$.

The jump matrix for the RH problem in this region, after applying the conjugation as in the collisionless shock region, is of the form (38). Note that (48), along with the fact that

$$t\big|g^+(z)+g^-(z)\big|\le|f(n,t)| \quad \text{for} \quad z\in\big(\alpha,\alpha^{-1}\big)_{\mathrm{arc}}\,,$$

implies that oscillation in the off-diagonal entries of the jump matrix are controlled on $\big(\beta,\beta^{-1}\big)_{\mathrm{arc}}$. To analyze the situation concerning the diagonal entries, define $h(n,t)$ by

$$\frac{h(n,t)}{t}=\int_\alpha^\beta\frac{1}{p^2}\sqrt{(p-\alpha)\left(p-\alpha^{-1}\right)(p-\beta)\left(p-\beta^{-1}\right)}^{+}\,dp.$$

Then $t\big|g^+(z)-g^-(z)\big|\le|h(n,t)|$ for $z\in(\beta,\alpha)_{\mathrm{arc}}$. Using the change of variables $z(k)=K^{-1}(k)$ given in (41), one can see that there exists a constant $C>1$ such that

$$\frac{1}{C}\le\frac{f(n,t)}{t\rho_0^3}+\frac{h(n,t)}{t\rho_0^3}\le C$$

in this region, where $\rho_0=\operatorname{Im}z_0$ as before. Now note that

$$t\rho_0^3\sim t\sqrt{8}\left(1-\frac{t-t^{1/3}r(t)}{t}\right)^{3/2}=t\sqrt{8}t^{-1}r(t)^{3/2}=\sqrt{8}r(t)^{3/2}\to\infty,\quad\text{as}\quad t\to\infty.$$

by the assumptions on $r(t)$. This implies that

$$\frac{f(n,t)}{t\rho_0^3}\to0\quad\text{as}\quad t\to\infty,$$

and (47) is solvable for sufficiently large t. Furthermore,

$$h(n,t)\sim Ct\rho_0^3\to\infty\quad\text{as}\quad t\to\infty,$$

which implies that the $(2,2)$-entries of the jump matrix given in (38) all tend to 0 as $t\to\infty$ in this region.

We now examine

$$\left[1-R(z)R\left(z^{-1}\right)\right]e^{h(n,t)}\quad\text{on}\quad\left(\beta,\beta^{-1}\right)_{\mathrm{arc}}\,, \tag{49}$$

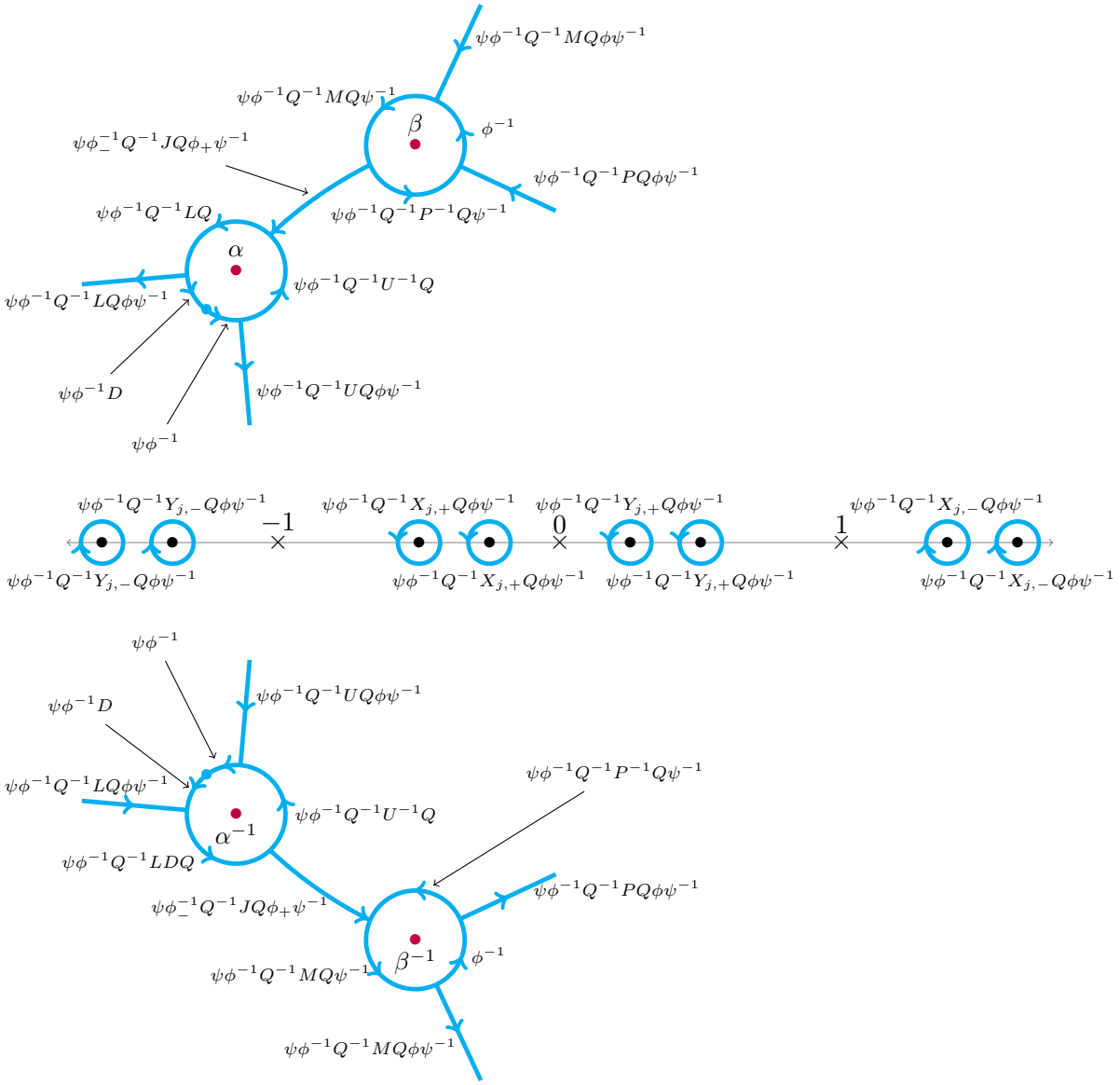

FIGURE 13. A zoomed view of the jump contours and matrices of the final deformation of the RH problem in the collisionless shock region. Note that ϕ and ψ commute.

using the change of variables $z(k) = K^{-1}(k)$.

$$\left[1 - R\big(z(k)\big)R\big(z(k)^{-1}\big)\right] e^{h(n,t)} = \nu\big(z(k)+1\big)^2\big(1+\mathcal{O}(z(k)+1)^2\big)e^{h(n,t)} = \nu\rho_0^2\left(1+\mathcal{O}\left(\rho_0^2\right)\right)e^{h(n,t)} \tag{50}$$

uniformly in k for A and B bounded as $t \to \infty$. Thus we are led to examine the behavior of $\rho_0^2 e^{h(n,t)}$ for large values of $t > 0$. Note that $h(n,t) = \mathcal{O}(r(t)^{3/2})$, $\rho_0^2 = \mathcal{O}(t^{-2/3}r(t))$, and that for any $c > 0$ there exists T such that $r(t)^{3/2} \le c\log(t)$ for $t > T$. There exists C_1, $C_2 > 0$

$$\rho_0^2 e^{h(n,t)} \le C_1 t^{-2/3} r(t) e^{C_2 c \log t} \le C_1 t^{-2/3} t^{C_2 c} r(t) \to 0, \quad \text{as} \quad t \to \infty, \tag{51}$$

for c chosen sufficiently small. This implies that the $(1,1)$-entries of the jump matrix all tend to zero. Therefore the entries of the jump matrix remain bounded and this gives us an asymptotically well-behaved RH problem without any lensing on $\left[\beta, \beta^{-1}\right]_{\text{arc}}$. After lensing on $\mathbb{T} \setminus \left[\beta, \beta^{-1}\right]_{\text{arc}}$ we obtain an RH problem for $\Phi_{1,\text{t}}$, see Figure 14. Defining $\Phi_{2,\text{t}} = \Phi_{1,\text{t}}\phi$, we present the jump contours and the jump matrices for $\Phi_{2,\text{t}}$ near α^{-1} and β^{-1} in Figure 15.

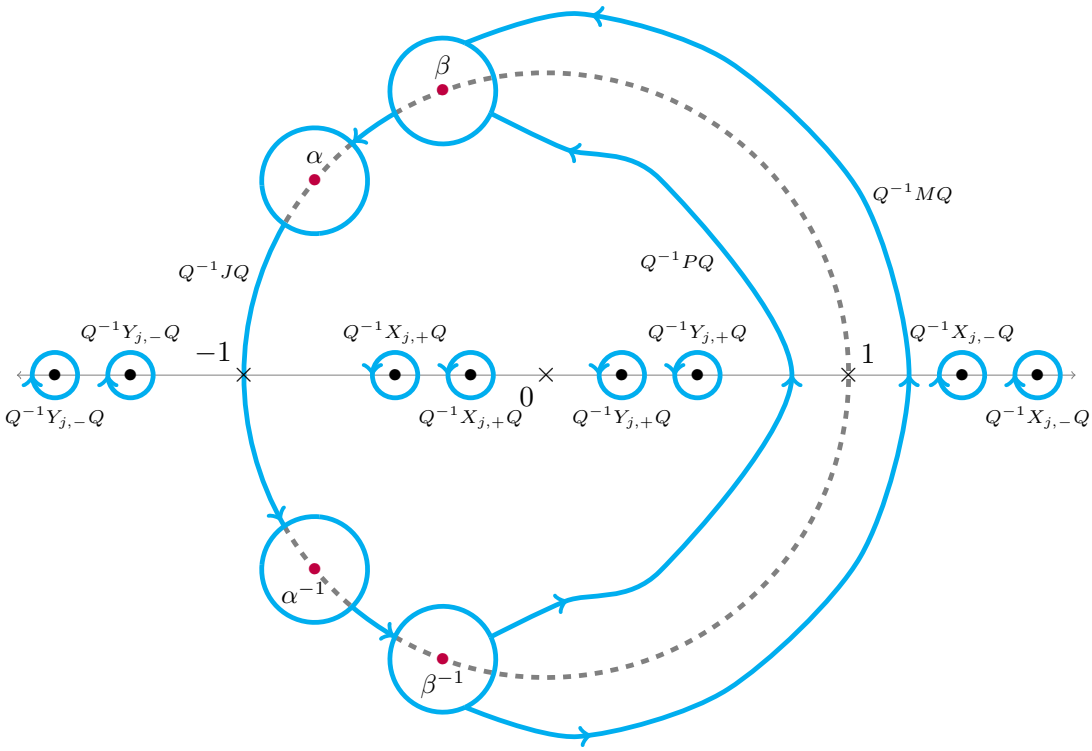

(a)

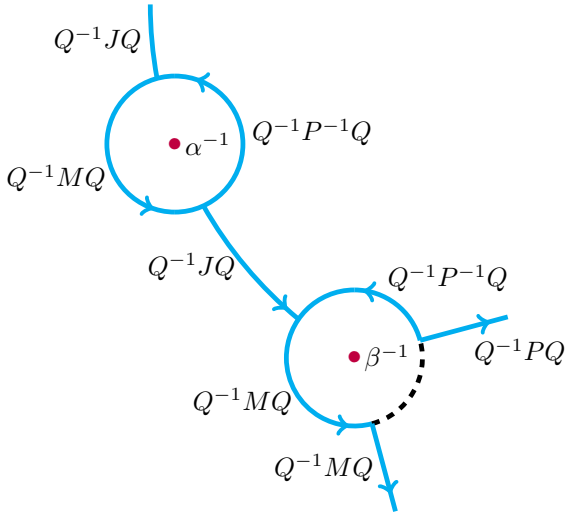

(b)

FIGURE 14. (a) The initial deformation of the RH problem in the transition region region for a function $\Phi_{1,\mathrm{t}}$, (b) The initial jump contours and matrices near α^{-1}, β^{-1}.

Finally, define

$$\Phi_{3,\mathrm{t}}(z) = \begin{cases} \Phi_{2,\mathrm{t}}(z)\phi^{-1}(z), & \text{inside the circles centered at } \alpha^{\pm 1} \text{ and } \beta^{\pm 1}, \\ \Phi_{2,\mathrm{t}}(z), & \text{otherwise.} \end{cases}$$

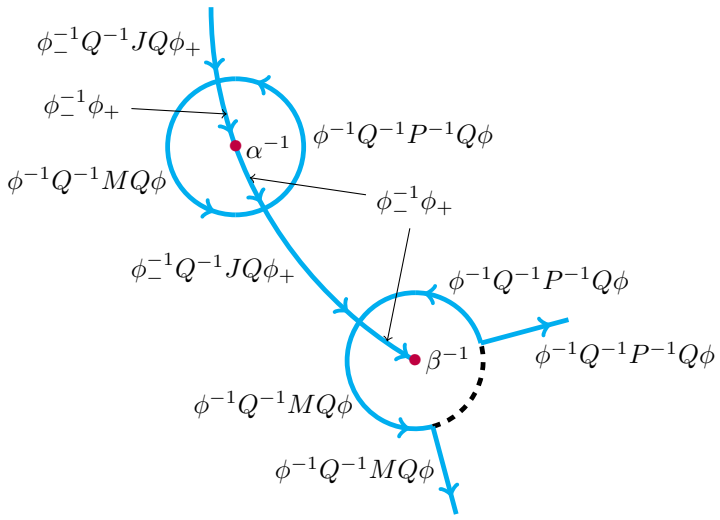

FIGURE 15. The jump contours and matrices for $\Phi_{2,\mathfrak{t}}$ near α^{-1}, β^{-1}.

The jump contours and the jump matrices for the final RH problem (for $\Phi_{3,\mathfrak{t}}$) is given in Figure 16. The scaling of the circles around α, β, α^{-1} and β is the same as in the collisionless shock region: $\propto t^{-2/3}$.

Remark 4.1. In the collisionless shock region when $\mathfrak{t} := -\frac{\log \rho_0^2}{t\rho_0^3} \approx 0$, $\alpha \approx \beta$ and the g function is essentially zero. This is the degeneration of the collisionless shock region to the dispersive region and hence the two regions overlap. The transition from the collisionless shock region to the transition region an be seen as $t \to \infty$, when

$$\mathfrak{t} = -i\int_B^A \frac{\sqrt{(q-A)(q-B)\left(q+\bar{A}\right)\left(q+\bar{B}\right)}^+}{(\lambda_0 - i\rho_0 q)^2}\, dq \approx -i\int_B^A \sqrt{(q-A)(q-B)\left(q+\bar{A}\right)\left(q+\bar{B}\right)}^+\, dq,$$

and $A \approx 0$ (see Appendix C.2 for the definition of A and B). This occurs when $n = t - C_1 t^{1/3}(\log t)^{2/3}$ as $C_1 \downarrow 0$ and it can been seen that the jump matrices in the transition region are regularized for $r(t) = \epsilon(\log t)^{2/3}$ for ϵ sufficiently small. Thus the collisionless shock region and the transition region overlap. In the transition region as $t \to \infty$ we have

$$\frac{f(n,t)}{t\rho_0^3} = -\int_A^0 \frac{\sqrt{(q-A)(q-B)\left(q+\bar{A}\right)\left(q+\bar{B}\right)}}{(\lambda_0 - i\rho_0 q)^2}\, dq \approx \int_0^A \sqrt{(q-A)(q-B)\left(q+\bar{A}\right)\left(q+\bar{B}\right)}\, dq.$$

Thus for $f(n,t)/(t\rho_0^3)$ sufficiently small, this equation is solvable for A. Then note that for $n = t - c_3 t^{1/3}$, $t\rho^3 \sim (2c_3)^{3/2}$. Thus choosing c_3 sufficiently large, we see that the Painlevé region and the transition region overlap and the g-function degenerates to zero as $A \to 0$ (or $\alpha \to -1$). In this way, our deformations can be seen to bridge all regions.

4.5. **The Soliton Region.** In this region, we have $|n| > t$. Therefore, the stationary phase points are no longer on the unit circle. Instead, for $n > 0$:

$$z_0 = -\frac{n}{t} + \sqrt{\left(\frac{n}{t}\right)^2 - 1} \in (-1, 0)\,,$$

and hence $z_0^{-1} \in (-\infty, -1)$. We use $J = MP$ decomposition within the strip of analyticity for the reflection coefficient and make the deformed contours (for the jumps M and P) pass through the stationary phase points as long as they remain inside the strip of analyticity. Once $z_0^{\pm 1}$ leave the strip, the deformed contours truncate to two circles: one enclosed by the unit circle, other enclosing the unit circle. More precisely, let $\mathcal{A}_\nu = \left\{z = re^{i\omega} \colon \omega \in [0, 2\pi),\ r \in (1-\nu, 1+\nu)\right\}$, $\nu > 0$, be the strip where $R(z)$ is analytic. Choose $r \in (0,1)$ that satisfies

$$1 - r = \min\left\{|z_0 + 1|, \frac{\nu}{2}\right\}.$$

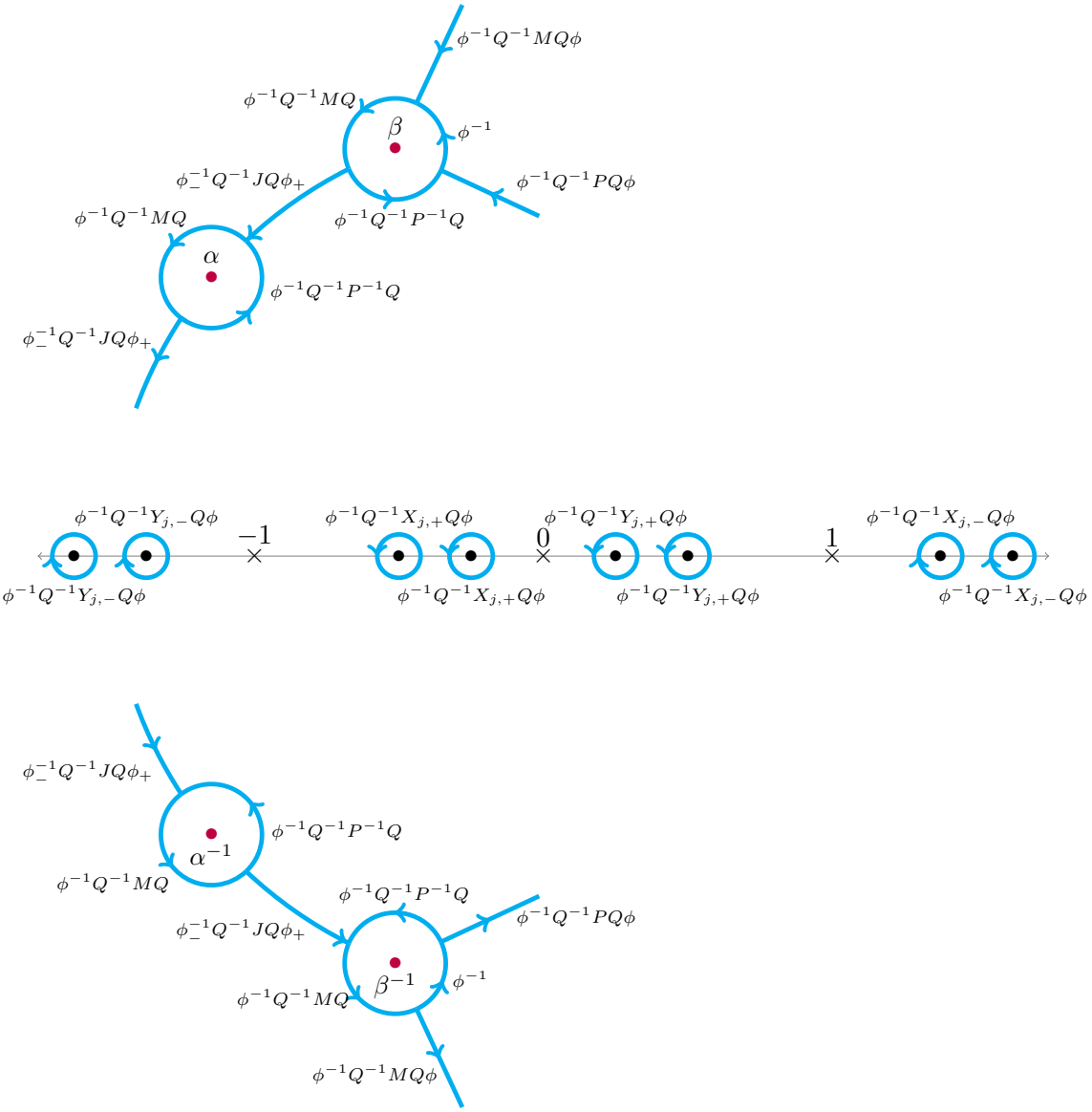

FIGURE 16. A zoomed view of the jump contours and matrices of the final deformation of the RH problem (for $\Phi_{3,\mathrm{t}}$) in the transition region.

As in the dispersive region, we use the jump

$$M(z;n,t) = \begin{pmatrix} 1 & -R\left(z^{-1}\right)e^{-\theta(z;n,t)} \\ 0 & 1 \end{pmatrix}$$

on the circle Γ_- which is centered at $z=0$ with radius $1/r$, and

$$P(z;n,t) = \begin{pmatrix} 1 & 0 \\ R(z)e^{\theta(z;n,t)} & 1 \end{pmatrix}$$

on the circle Γ_+ which is centered at $z=0$ with radius r. Now, define $\zeta_0 \in (-1,0)$ by $\operatorname{Re}\theta(z;n,t)=0$, that is, by

$$\frac{n}{t} = -\frac{\zeta_0 - \zeta_0^{-1}}{2\log|\zeta_0|}\,.$$

For $n > t > 0$, $z_0 < \zeta_0$ (see [18]). Thus, the choice of r ensures that $\Gamma_\pm \subset \mathcal{A}_\nu$ and that the exponents in P and M have negative real parts on their domains. Consequently, P and M tend to I exponentially fast as $t \to \infty$. The strip of analyticity, jump matrices, and jump contours for the RH problem in this region are presented in 17 in absence of poles. When poles are present, the choice of r is further restricted to make sure

that the contours do not intersect with the circles, $D_j^{\pm}$, around each pole, $\zeta_j^{\pm 1}$, $j = 1, 2, \dots, N$. We use the jumps $X_j^{\pm}$ and $Y_j^{\pm}$ (defined in (31) and (32)) on $D_j^{\pm}$ precisely as described in Section 4.1.

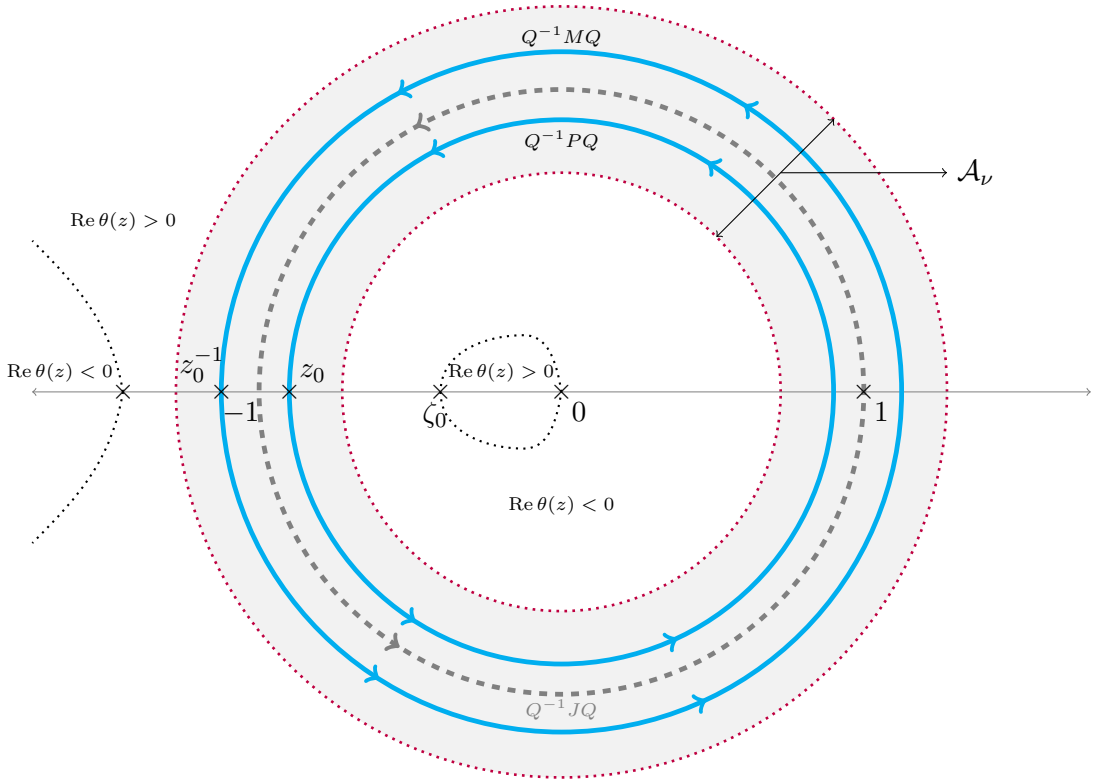

FIGURE 17. The jump contours and matrices for the RH problem in the soliton region.

5. Numerical results

5.1. **Direct scattering.** In this section we present some numerical results on the computation of the scattering data. We study two choices of initial data in detail:

(TS) A choice of initial data giving rise to two solitons (TS) is

$$a_n(0) = \frac{1}{2} + \frac{4}{5} n e^{-n^2},$$
$$b_n(0) = \frac{1}{10} \operatorname{sech}(n).$$

(NS) A choice of non-solitonic (NS) (*i.e.*, $\sigma_{\mathrm{pp}}(L) = \varnothing$) initial data is

$$a_n(0) = \frac{1}{2} - \frac{1}{4} e^{-n^2},$$
$$b_n(0) = \frac{1}{10} \operatorname{sech}(n).$$

The reflection coefficient on $\mathbb{T}$ is shown in Figure 18(a) for TS initial data and in Figure 18(b) for NS initial data. With K in Section 3 sufficiently large ($K = 30$ is sufficient), accuracy is guaranteed. In the case of the TS data, we find

$$(\zeta_1, \zeta_2) \approx (0.596142, -0.704859),$$
$$(\gamma_1, \gamma_2) \approx (3.25791, 1.43054).$$

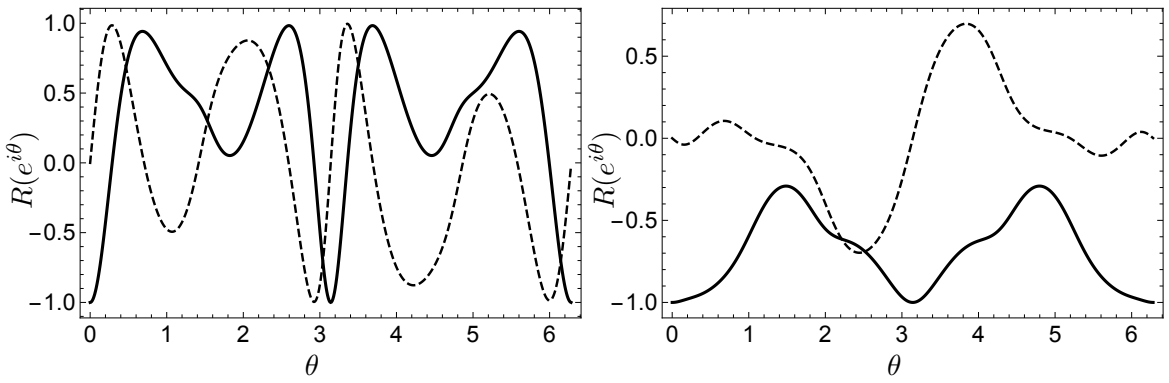

FIGURE 18. Numerical computation of the reflection coefficient $R(z)$ ($\operatorname{Re} R(z)$ solid curve, $\operatorname{Im} R(z)$ dashed graph) with initial data where (a) two eigenvalues are present (TS) and (b) $\sigma_{\mathrm{pp}}(L)$ is empty (NS).

5.2. **Inverse scattering.** In this section we present numerical results for the computation of the inverse scattering transform. These results are of three flavors:

- Example solution plots,
- error analysis, and
- numerical asymptotics.

5.2.1. *Example solutions.* Here we present plots of the solution of the Toda lattice with both TS and NS initial data. See Figures 19 and 20 for plots of $a_n(t)$ and $b_n(t)$ when $t = 100, 1000$ in the case of TS initial data. Two solitons traveling in opposite directions are clearly visible. Indeed, this is anticipated because ζ_1 and ζ_2 have opposite signs. See Figures 21 and 22 for plots of $a_n(t)$ and $b_n(t)$ when $t = 100, 1000, 10000$ in the case of NS initial data. As stated above, no solitons are present in the solution and the high oscillation in the solution is apparent, especially at $t = 10000$.

5.2.2. *Error analysis.* To examine the accuracy of our numerical IST *a posteriori* we compare it with a naive time-stepping method. A more detailed description of the method can be found in [4]. Fix $K > 0$ and consider the Toda lattice with Dirichlet boundary conditions: $a_{-K}(t) = a_K(t) = 1/2$, $b_{-K} = b_K = 0$. Here K is chosen sufficiently large so that the solution remains flat at the boundary $\pm K$ for all times simulated. If $t < T$, it suffices to take $K = cT$ for some $c > 1$ which is larger than the speed of the fastest soliton present in the solution. This is a finite-dimensional system of ODEs and can be integrated in time using the fourth-order Runge–Kutta method. We compare the time-stepped solution at $t = 30$ with $\Delta t = 10^{-5}$ with the solution computed via the inverse scattering transform in Figure 23. As the number of collocation points in increased, the numerical inverse scattering solution converges exponentially to the true solution, with these errors saturating at approximately 10^{-11}. It is reasonable to expect that at this point the numerical IST gives a more accurate solution than the time-stepping method. Furthermore, on a standard laptop it takes ≈ 6 seconds to compute the solution at $t = 30$, $n = 30$ with 720 collocation points using the IST and $\approx 2 \times 10^5$ seconds with the naive time-stepping method[5]. This comparison is pessimistic as contour truncation (see Figure 24 and the next paragraph) reduces IST computation times as t increases while time-stepping methods see their complexity increase.

We emphasize that the number of collocation points required to solve the Toda lattice using the numerical inverse scattering transform to a given accuracy is typically decreasing with respect to t. This is because the deformations performed on the original RH problem force some contours to tend exponentially fast to the identity matrix as t increases. Thus, after truncation, discussed in Section 2.5, fewer contours need to be discretized in the RH problem resulting in fewer collocation points. To see this in action, using the contour

[5]It should be noted that the time-stepping method produces an approximation of the entire solution profile in this time while the numerical IST gives the solution at only one point. Even so, it would take $\approx 1.2 \times 10^4$ second to compute the entire solution profile at this rate with the numerical IST.

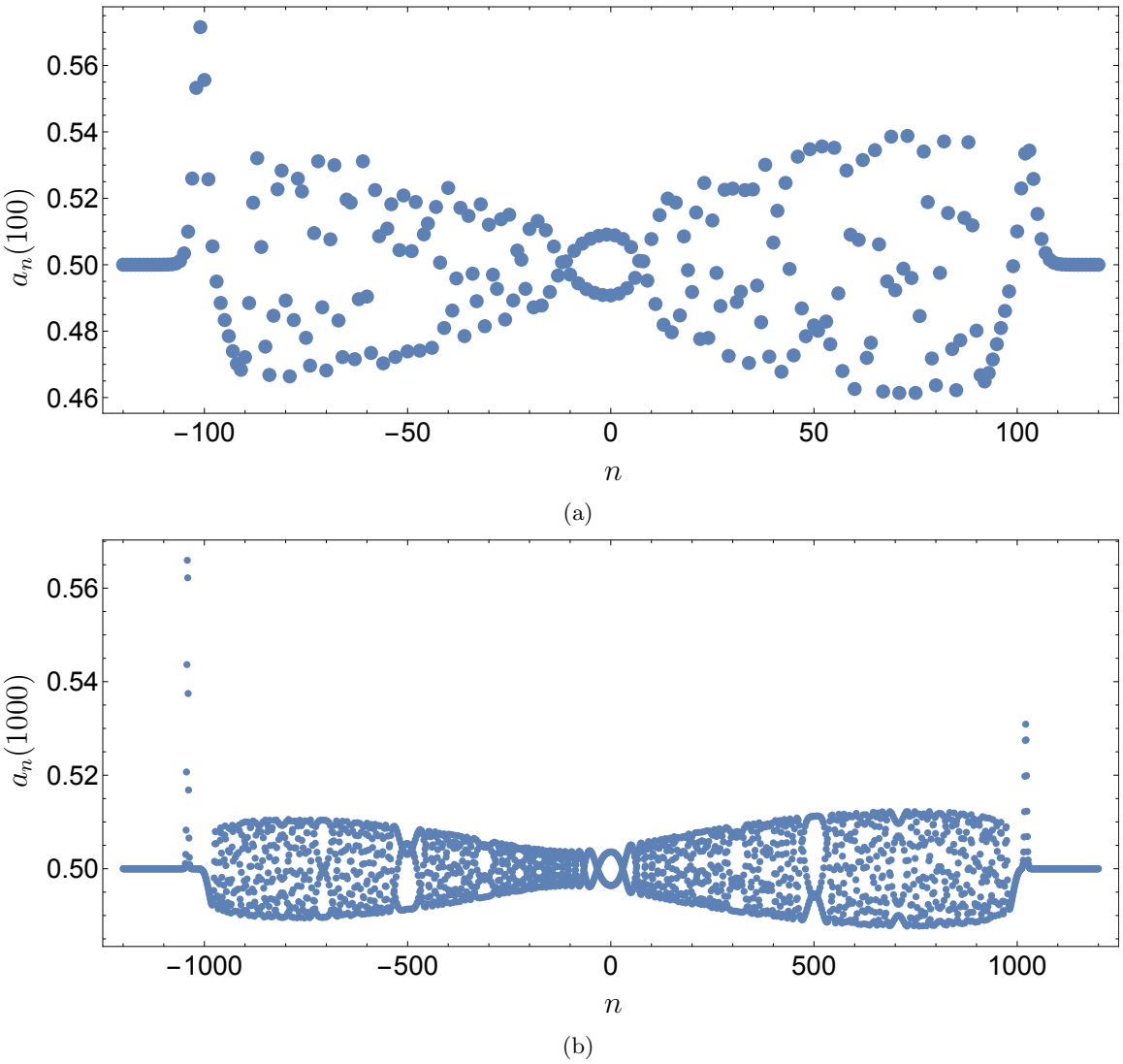

FIGURE 19. Solution $a_n(t)$ obtained by numerical inverse scattering (a) at $t = 100$, (b) at $t = 1000$. The horizontal axis denotes the spatial parameter $n \in \mathbb{Z}$. The initial data produces two eigenvalues on opposite sides of the a.c.-spectrum giving rise to two solitons traveling in opposite directions.

truncation algorithm described in [37], see Figure 24. Thus the errors seen in Figure 23 are pessimistic for large values of t.

5.2.3. *Numerical asymptotics.* We have seen that the accuracy of the numerical method is easily verified for short/moderate times by the comparison with time stepping methods. Thus in terms of accuracy, the method will also out-perform the asymptotic formulae ([30, 29, 16]) for long-time. Thus, with a numerical inverse scattering transform the numerical evaluation of asymptotic formulae (which is truly a non-trivial task) is obsolete. To demonstrate this, we show the long-time behavior of the solution with NS initial data in the dispersive, Painlevé and collisionless shock regions. We call such computations *numerical asymptotics*.

- Dispersive region.
  To show the solution in the dispersive region we let n depend on t through $n = \lfloor 7t/10 \rfloor$ where $\lfloor \cdot \rfloor$ represents the integer part. See Figure 25 for a plot of the solution into the dispersive region.
- Painlevé region.
  To show the solution in the Painlevé region we let n depend on t through $n = \lfloor t - t^{1/3} \rfloor$. See Figure 26 for a plot of the solution into the Painlevé region.

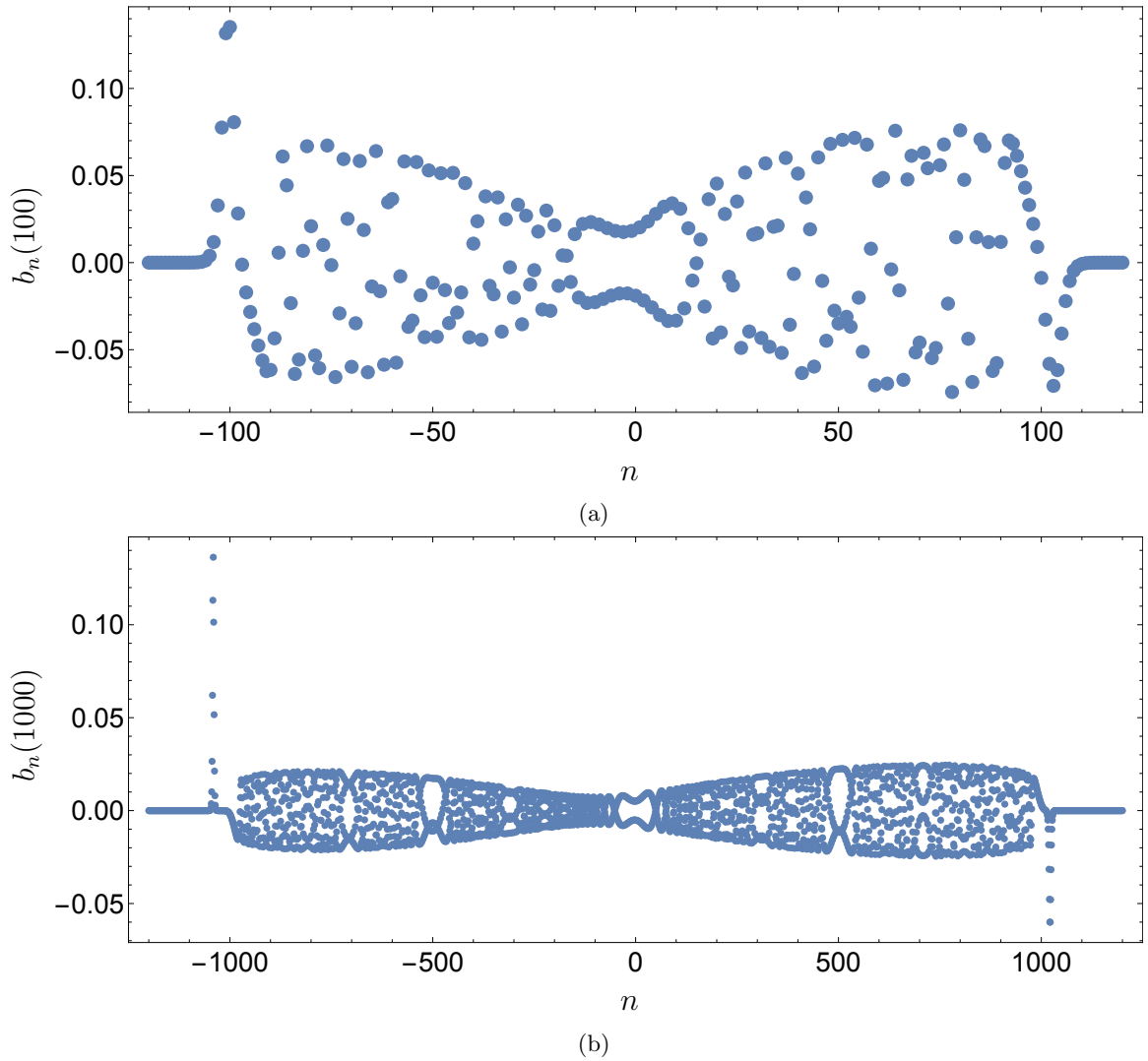

FIGURE 20. Solution $b_n(t)$ obtained by numerical inverse scattering (a) at $t = 100$, (b) at $t = 1000$. The horizontal axis denotes the spatial parameter $n \in \mathbb{Z}$. The initial data produces two eigenvalues on opposite sides of the a.c.-spectrum giving rise to two solitons traveling in opposite directions.

- Collisionless shock region.
  To show the solution in the collisionless shock region we let n depend on t through $n = \lfloor t - t^{1/3}(\log t)^{2/3} \rfloor$. See Figure 27 for a plot of the solution into the collisionless shock region.

APPENDIX A. SOLVING THE SINGULAR DIAGONAL RH PROBLEMS

There are two diagonal RH problems that must be solved, and computed numerically, in our deformation procedures. The Δ first is (34) and the second is ψ in (42). Note that because $g^+(z) - g^-(z)$ is constant for $z \in \left(\alpha, \alpha^{-1}\right)_{\text{arc}}$, these problems are both of the form

$$\begin{aligned} &\mathcal{X}^+(z) = \mathcal{X}^-(z) \begin{pmatrix} c\tau(z) & 0 \\ 0 & (c\tau(z))^{-1} \end{pmatrix}, \ z \in (\gamma, \gamma^{-1}), \ |\gamma| = 1, \ \operatorname{Im}\gamma > 0, \\ &\mathcal{X}(\infty) = I, \end{aligned}$$

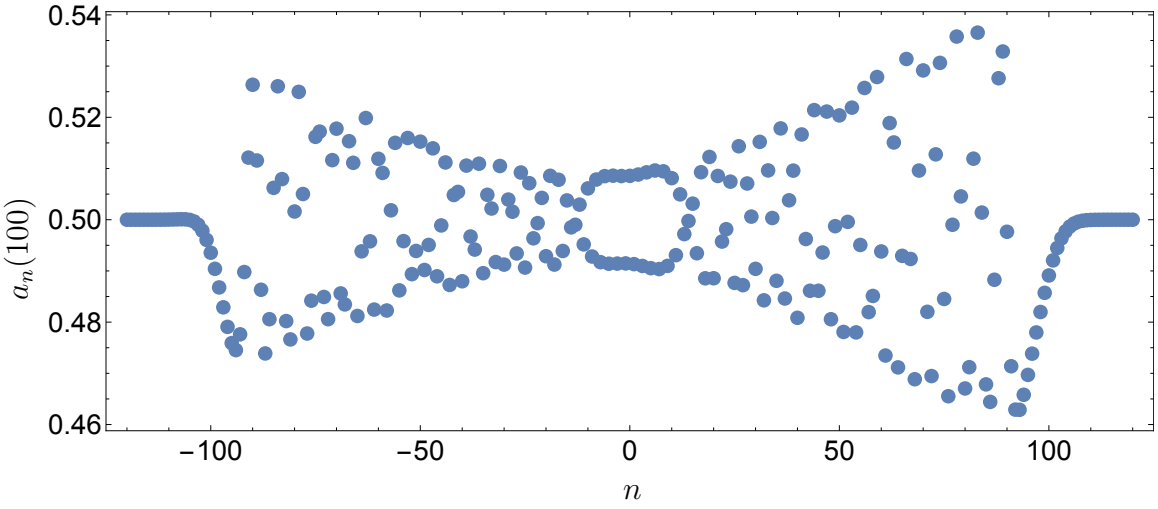

(a)

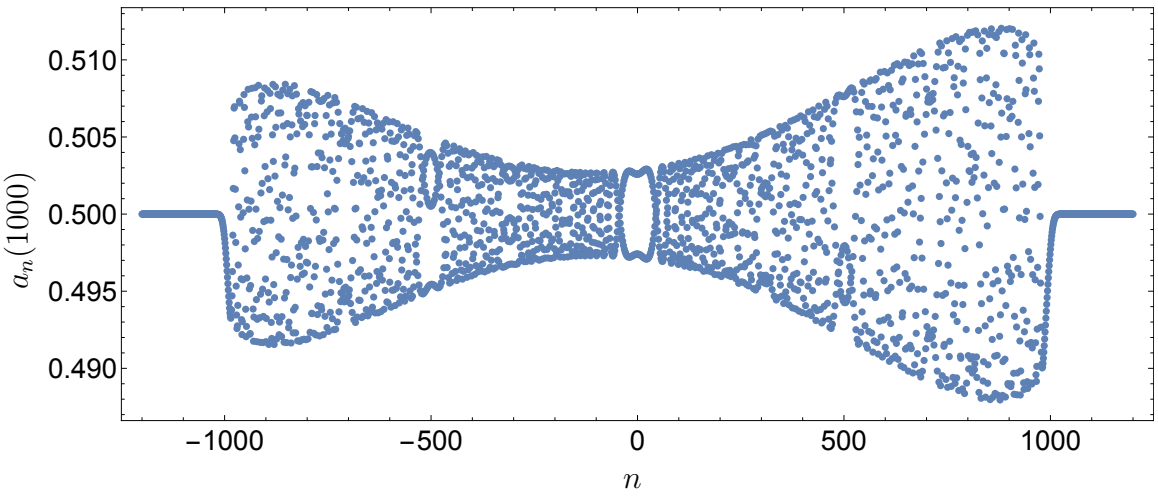

(b)

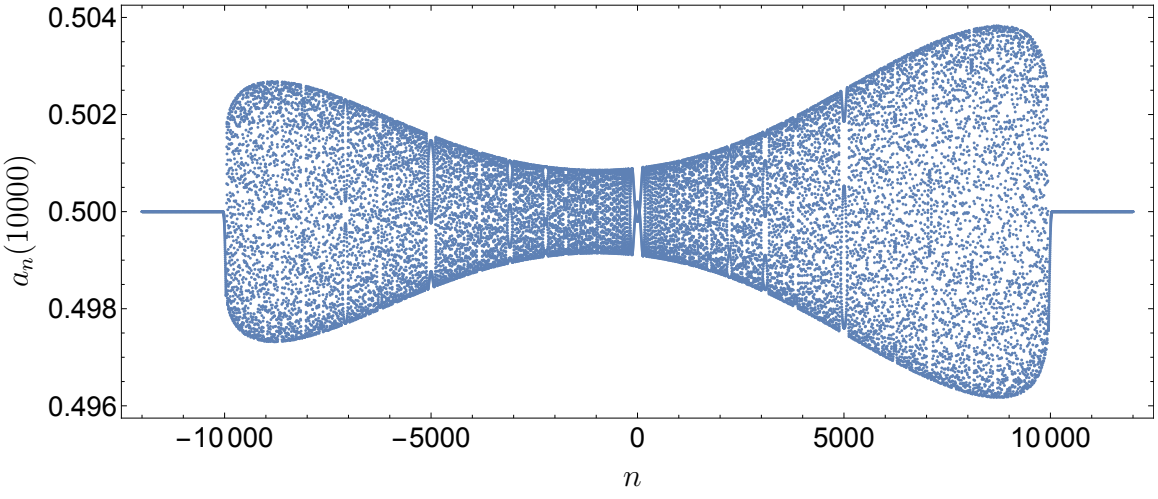

(c)

FIGURE 21. Solution $a_n(t)$ obtained by numerical inverse scattering (a) at $t = 100$, (b) at $t = 1000$, (b) at $t = 10000$. The horizontal axis denotes the spatial parameter $n \in \mathbb{Z}$. The initial data produces no eigenvalues and therefore no solitons are present in the solution.

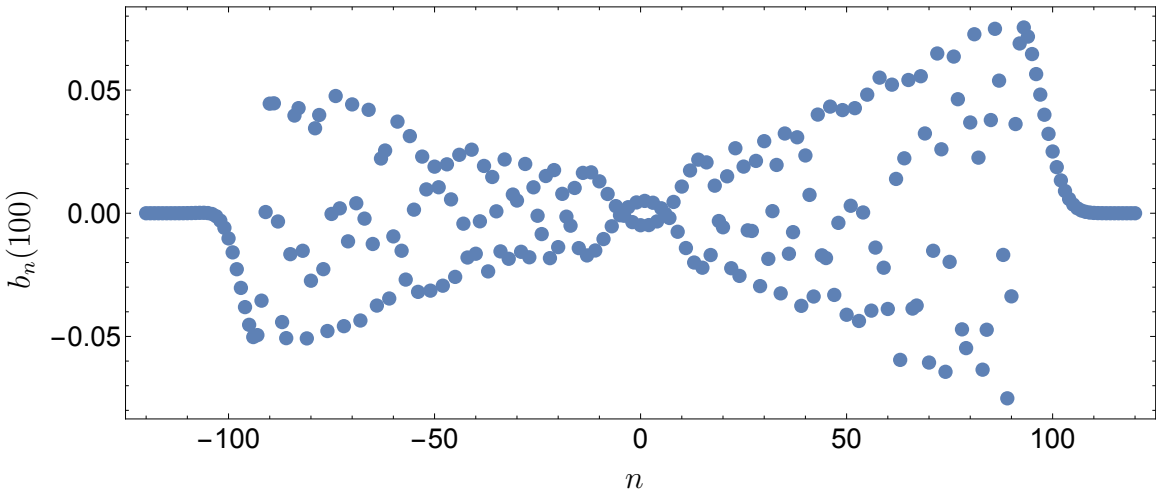

(a)

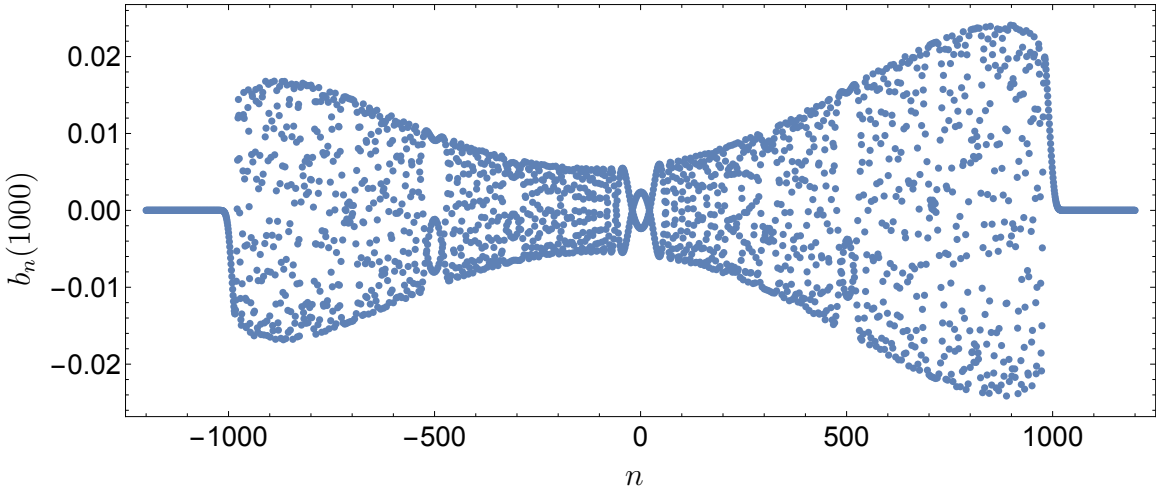

(b)

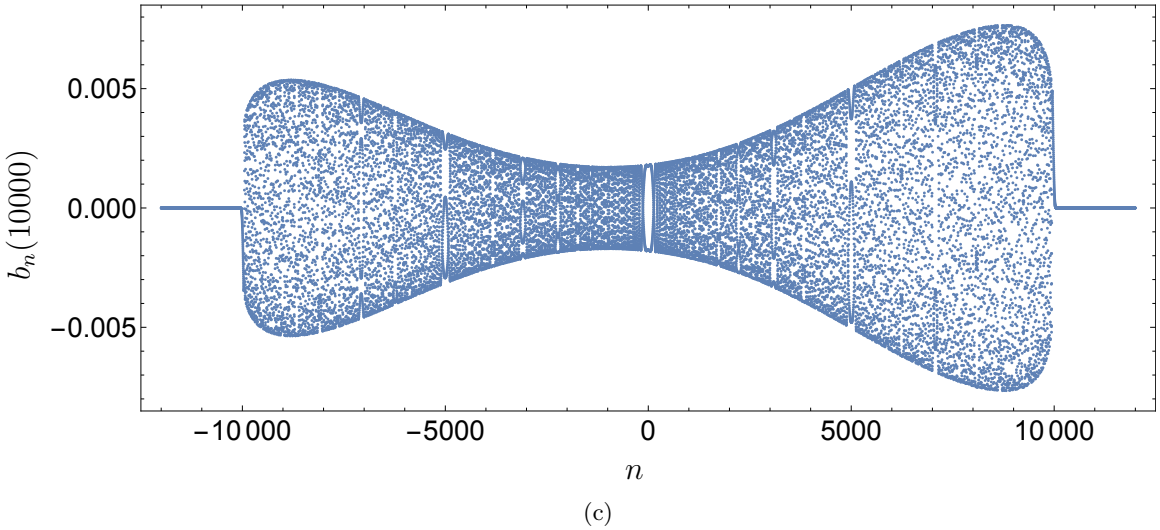

(c)

FIGURE 22. Solution $a_n(t)$ obtained by numerical inverse scattering (a) at $t = 100$, (b) at $t = 1000$, (b) at $t = 10000$. The horizontal axis denotes the spatial parameter $n \in \mathbb{Z}$. The initial data produces no eigenvalues and therefore no solitons are present in the solution.

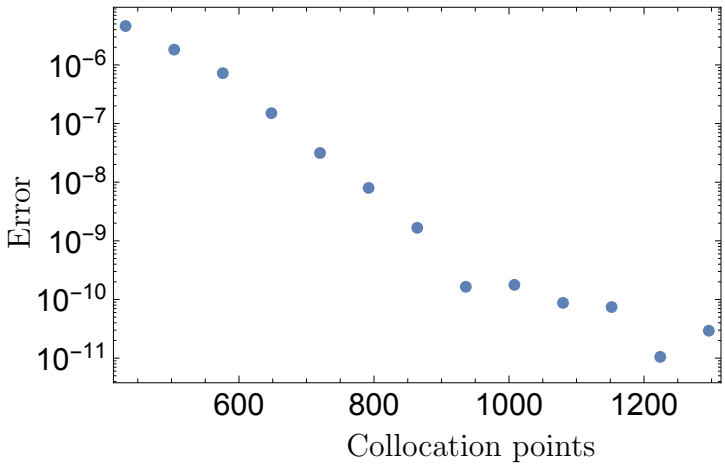

FIGURE 23. The error between a solution of the Toda lattice computed using time steeping and numerical inverse scattering. The error shown is the maximum of the error computed at the points $(n,t) = (-51,30),(-31,30),(-11,30)$ plotted versus the number of collocation points used in the numerical solution of the associated RH problem.

for a positive real constant c. It follows from classical theory that $\mathcal{X}_{12} \equiv \mathcal{X}_{21} \equiv 0$, $\mathcal{X}_{11}(z) = 1/\mathcal{X}_{12}(z)$. From this

$$\mathcal{X}_{11}(z) = \exp\left(\frac{1}{2\pi i}\int_{(\gamma,\gamma^{-1})_{\text{arc}}} \frac{\log(c\tau(s))}{s-z} ds\right).$$

Furthermore, because $\log(c\tau(s))$ it follows that $\mathcal{X}_{11}(z)$ is bounded near γ and γ^{-1}, see [19]. The difficulty here is evaluating this numerically because $\log\tau(s)$ is singular at $s=-1$. We regularize the integrand by considering[6]

$$\tilde{\tau}(z) = -\frac{\tau(z)}{(z-z^{-1})^2} > 0,\ z \in \left(\gamma,\gamma^{-1}\right)_{\text{arc}},$$

so that the Cauchy integral of the smooth function $\log\tilde{\tau}(z)$ along (γ,γ^{-1}) can be computed with the methods referenced in Section 2.5. It follows that

$$\mathcal{I}(z;\gamma) = \frac{1}{2\pi i}\int_{(\gamma,\gamma^{-1})_{\text{arc}}} \frac{2\log(s-s^{-1})}{s-z} ds = \frac{1}{\pi i}\int_{(\gamma,\gamma^{-1})_{\text{arc}}} \frac{\log(s+1)}{s-z} ds + \frac{1}{\pi i}\int_{(\gamma,\gamma^{-1})_{\text{arc}}} \frac{\log(1-s^{-1})}{s-z} ds.$$

We note that $\log(1-z^{-1})$ has its branch cut on $[0,1]$ so that it is smooth on (γ,γ^{-1}) and its Cauchy integral can be, again, computed with the methods referenced in Section 2.5. Thus it remains to calculate by Cauchy's integral formula

$$\frac{1}{2\pi i}\int_{(\gamma,\gamma^{-1})_{\text{arc}}} \frac{2\log(s+1)}{s-z} ds = \frac{1}{2\pi i}\int_{I_\gamma} \frac{2\log(s+1)}{s-z} ds + \begin{cases} 0, & \text{if } \in D_\gamma^c, \\ 2\log(z+1), & \text{if } z \in D_\gamma, \end{cases}$$

where I_γ is the vertical line connecting γ and γ^{-1} with downward orientation and D_γ is the region enclosed by I_γ and $\left(\gamma,\gamma^{-1}\right)_{\text{arc}}$. It turns out that

$$\frac{1}{2\pi i}\int_{I_\gamma} \frac{2\log(s+1)}{s-z} ds = \frac{1}{2\pi i}\left(\log(1+\gamma^{-1})\log\left(\frac{z-\gamma^{-1}}{1+z}\right) - \log(1+\gamma)\log\left(\frac{z-\gamma}{1+z}\right)\right.$$
$$\left. + \text{Li}_2\left(\frac{1+\gamma^{-1}}{1+z}\right) - \text{Li}_2\left(\frac{1+\gamma}{1+z}\right)\right)$$

[6]As the amplitude of the initial data increases, $\tilde{\tau}(\pm 1)$ approaches zero. Round-off error that is amplified by forming the ratio may become significant and degrade the accuracy obtained in evaluating $\tilde{\tau}$. In this case, once should look for a different method to compute $\mathcal{X}_{11}$.

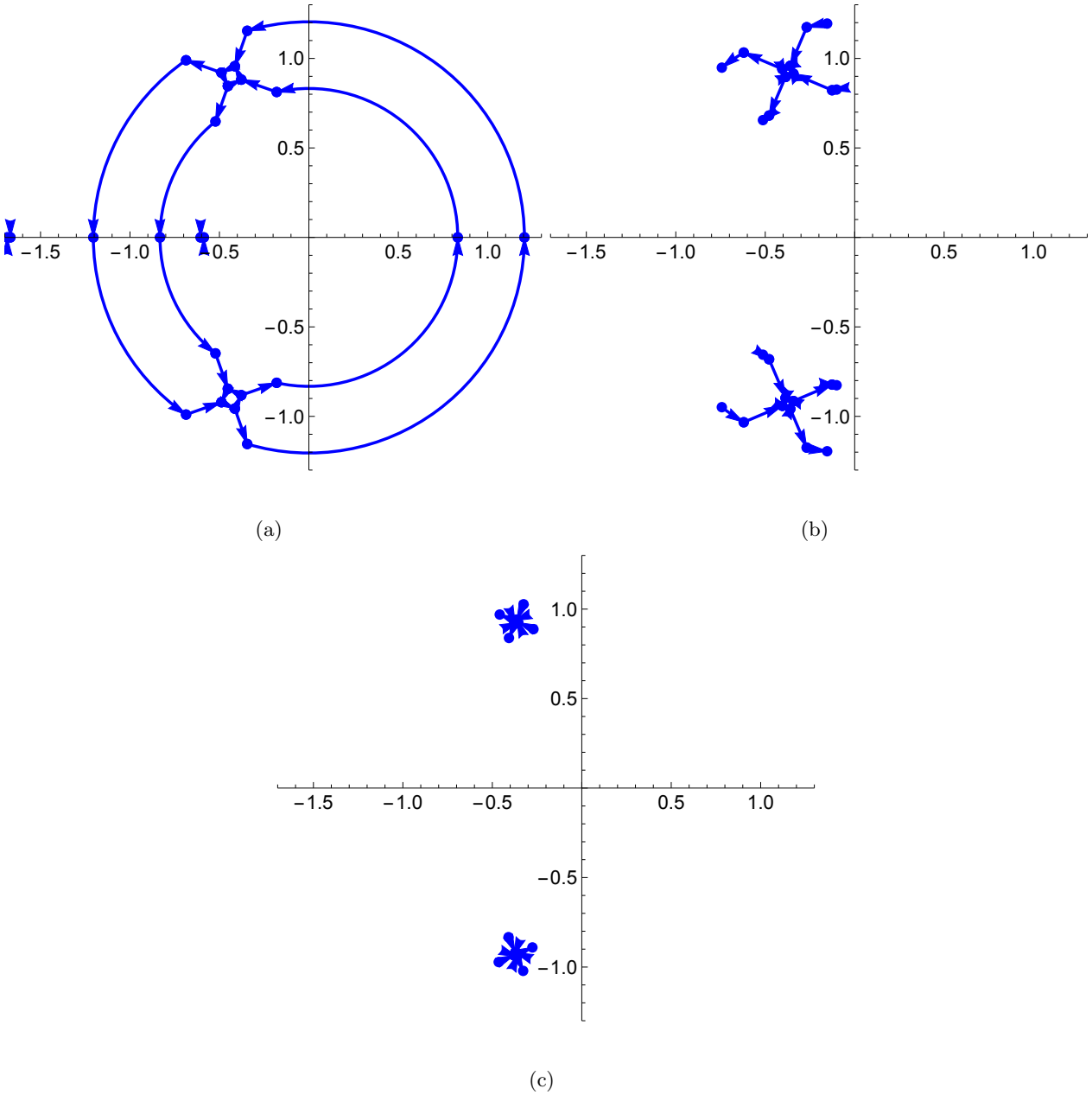

FIGURE 24. Contours used in numerical inverse scattering for the Toda lattice in the dispersive region with TS initial data. This figure shows how contour truncation localizes the contours as $t \to \infty$. (a) The contours for $(n,t) = (-11, 30)$ with 28 total contours. (b) The contours for $(n,t) = (-110, 300)$ with 24 total contours (soliton contours have been truncated). (c) The contours for $(n,t) = (-1100, 3000)$ with 14 total contours.

where Li_2 is the dilogarithm function, see [20, Section 25.12], with appropriately chosen branch cuts. Stock special function routines in `Mathematica` allow this function to be computed accurately. Then

$$\mathcal{X}_{11}(z) = \exp\left(\frac{1}{2\pi i}\int_{(\gamma,\gamma^{-1})_{\mathrm{arc}}} \frac{\log(c\tilde{\tau}(s))}{s-z} ds + \mathcal{I}(z;\gamma)\right).$$

APPENDIX B. ON COMPUTING EIGENVALUES OF L

In this section we present a case where we fail to capture all of the eigenvalues of L numerically by using conventional eigenvalue algorithms on finite, $K \times K$ truncations L_K of the doubly-infinite Jacobi matrix L.

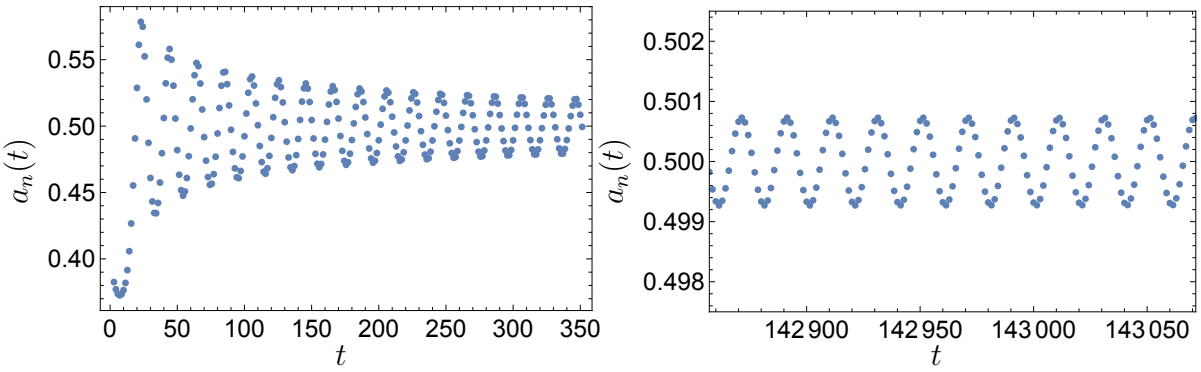

FIGURE 25. Numerical asymptotics in the dispersive region: $n = \lfloor 7t/10 \rfloor$. Such computations are accurate for arbitrarily large t.

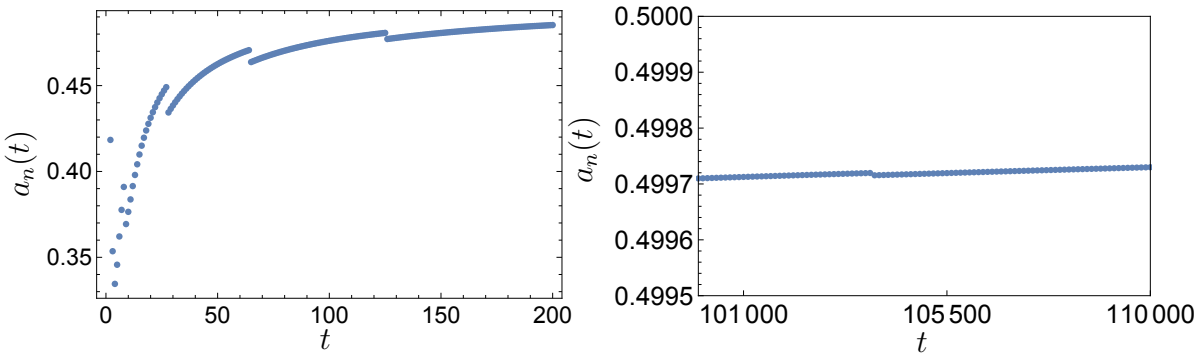

FIGURE 26. Numerical asymptotics in the Painlevé region: $n = \lfloor t - t^{1/3} \rfloor$. Such computations are accurate for arbitrarily large t

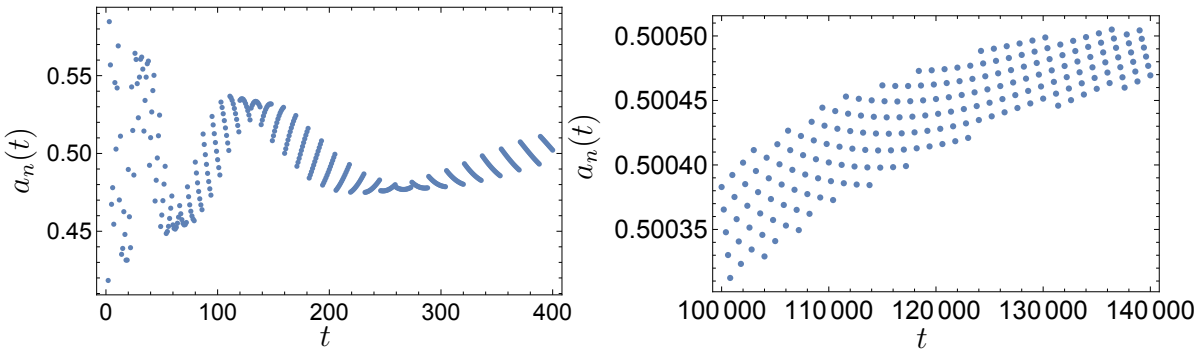

FIGURE 27. Numerical asymptotics in the collisionless shock region: $n = \lfloor t - t^{1/3}(\log t)^{2/3} \rfloor$. Such computations are accurate for arbitrarily large t.

For

$$\lambda_1^-(L) < \lambda_2^-(L) < \cdots < \lambda_{M^-}^- < -1 < 1 < \lambda_{M^+}^+ < \cdots < \lambda_2^+(L) < \lambda_1^+(L)$$

denote the eigenvalues of L. Note that the integers $M^\pm$ are finite for the Jacobi matrices that appear in this text, but they can be zero. Similarly, let

$$\lambda_1^-(L_K) < \lambda_2^-(L_K) < \cdots < \lambda_K^-(L_K) \quad \text{and} \quad \lambda_1^+(L_K) > \lambda_2^+(L_K) > \cdots > \lambda_K^+(L_K)$$

denote the real simple eigenvalues of any $K \times K$ truncation L_K, labeled in increasing (λ_j^-) and decreasing order (λ_j^+), respectively. Then

$$\begin{aligned} \lambda_j^-(L) &\leq \lambda_j^-(L_K) \quad \text{for } j = 1, 2, \ldots, \min\{M^-, K\}, \\ \lambda_j^+(L) &\geq \lambda_j^+(L_K) \quad \text{for } j = 1, 2, \ldots, \min\{M^+, K\}, \end{aligned}$$

and

$$\begin{aligned} -1 \le \lambda_j^-(L_K) \quad &\text{for } \min\{M^-, K\} < j \le K, \\ 1 \ge \lambda_j^+(L_K) \quad &\text{for } \min\{M^+, K\} < j \le K\,. \end{aligned}$$

In other words, pure point spectrum of L shrinks around the a.c.-spectrum under truncations. In particular, an eigenvalue of L that is close to the a.c.-spectrum might go inside the interval $\sigma_{\rm ac}(L) = [-1, 1]$ after applying a truncation, in which case it fails to be captured by conventional eigenvalue algorithms that are run on the finite truncations L_K. The example to be discussed below illustrates such a case. For a more detailed account on the spectra of finite truncations of doubly-infinite Jacobi matrices, we refer the reader to Section 4 in [4].

Consider the data $\{a_n^0, b_n^0\}$:

$$\begin{aligned} a_n^0 &= 1 - \frac{1}{2}\frac{\sqrt{\ell_{n-1}\ell_{n+1}}}{\ell_n}, \\ b_n^0 &= \frac{1}{2}(1 - 10^{-4})(z^* - 1/z^*)\left(\frac{\ell_n - 1}{\ell_n} - \frac{\ell_{n-1} - 1}{\ell_{n-1}}\right), \\ \ell_n &= 1 + e^{-4n/5}, \quad z^* = e^{-2/5}. \end{aligned} \tag{52}$$

which is created by inverting pure soliton initial data. Define the $2K+1 \times 2K+1$ truncation

$$L_{2K+1} = \begin{pmatrix} b_{-K} & a_{-K} & 0 & & & & \\ a_{-K} & b_{-K+1} & a_{-K+1} & \ddots & & & \\ 0 & a_{-K+1} & \ddots & \ddots & \ddots & & \\ & \ddots & \ddots & \ddots & a_{K-2} & 0 & \\ & & \ddots & a_{K-2} & b_{K-1} & a_{K-1} & \\ & & & 0 & a_{K-1} & b_K & \end{pmatrix},$$

for $K = 2400$. Using standard eigenvalue algorithms for tridiagonal symmetric matrices on L_{2K+1} yields no eigenvalues outside $[-1, 1]$. However, the transmission coefficient has a pole outside $[-1, 1]$, which can be captured by Newton iteration to find zeros of $1/R(z)$ and we find $R(z^*) = 0$ for $z^* \approx 0.99982297716$ which corresponds to an eigenvalue $\lambda \approx 1.00000001567$ of L. Naturally, such an eigenvalue is difficult to capture via truncations because it does not emerge until K is very large. See Figure B for a illustration of the zero.

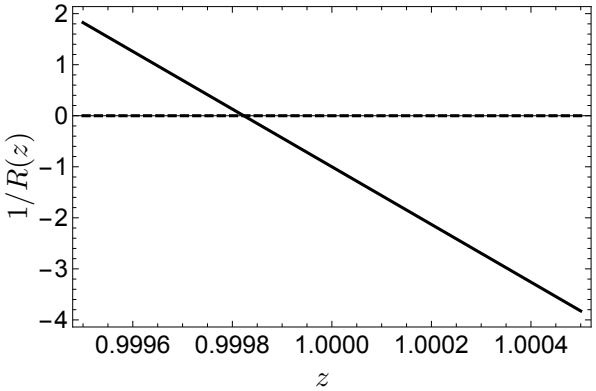

FIGURE 28. The reflection coefficient $R(z)$ for the initial data (52). A zero for $1/R(z)$ is observed near $z = 1$ corresponding to an eigenvalue of L. The zero is very close to the unit circle and therefore the corresponding eigenvalue is close to the right edge of the continuous spectrum of L. This eigenvalue is difficult to detect with traditional eigenvalue techniques but it is easily captured using the reflection coefficient.

APPENDIX C. TODA g-FUNCTION

In this section we explicitly define the g-function computed in Section 4.3. We use this form to determine the exact asymptotic form of the collisionless shock region and then discuss its computation.

C.1. **Construction of the Toda g-function.** Let $\lambda_0 < 0$ and $\rho_0 > 0$ denote the real and imaginary parts of the stationary point, z_0, respectively. For α, $\beta \in \mathbb{T}$ in the upper half-plane with $-1 \leq \operatorname{Re}\alpha \leq \lambda_0 \leq \operatorname{Re}\beta \leq 1$, define

$$F(\alpha,\beta) = \int_\beta^\alpha \frac{1}{p^2}\sqrt{(p-\alpha)\left(p-\alpha^{-1}\right)(p-\beta)\left(p-\beta^{-1}\right)}^+ dp.$$

Here the square root is defined with branch cuts on $[\beta,\alpha]_{\text{arc}}$ and $\left[\alpha^{-1},\beta^{-1}\right]_{\text{arc}}$ and asymptotics

$$\sqrt{(p-\alpha)\left(p-\alpha^{-1}\right)(p-\beta)\left(p-\beta^{-1}\right)} \sim p^2, \quad p\to\infty.$$

Lemma C.1. *Under the additional restriction* $\operatorname{Re}\alpha + \operatorname{Re}\beta = 2\lambda_0$, $F(\alpha,\beta) \in [0,4]$. *Moreover, for fixed* z_0, F *is a monotone decreasing function of* $\operatorname{Re}\alpha$ *as* $\operatorname{Re}\alpha$ *increases from* -1 *to* λ_0.

Proof. For notational simplicity set $\lambda_\alpha = \operatorname{Re}\alpha$, $\omega_\alpha = \arg\alpha$, and $\lambda_\beta = \operatorname{Re}\beta$, $\omega_\beta = \arg\beta$. Also, set

$$X(p) = \sqrt{(p-\alpha)\left(p-\alpha^{-1}\right)(p-\beta)\left(p-\beta^{-1}\right)}.$$

Then

$$F(\alpha,\beta) = \int_\beta^\alpha \frac{X^+(p)}{p}\frac{dp}{p},$$

First, note that

$$\left(\frac{X^+(p)}{p}\right)^2 = 4(z-\lambda_\alpha)(z-\lambda_\beta), \tag{53}$$

for $z = (p+p^{-1})/2$. Now, for p on the unit circle, $z = \operatorname{Re}p$ and the right hand side of (53) is negative in the domain of integration, vanishing only at $z=\lambda_\alpha$ and $z=\lambda_\beta$. This implies that $X^+(p)/p$ is purely imaginary.

Second, by definition $X(p)/p \sim p$ as $p\to\infty$ so that $\operatorname{Im}p > 0$ in the upper half-plane for $|p|$ large enough. We claim that $\operatorname{Im}(X(p)/p)$ cannot change sign outside the unit circle off the real axis. Suppose that it did. Then $X(p_*)/p_* = c$ would be real valued for some p_* with $|p_*| > 1$. For $z_* = (p_* + p_*^{-1})/2$

$$4(z_*-\lambda_\alpha)(z_*-\lambda_\beta) = c^2 \in \mathbb{R}. \tag{54}$$

Solving (54) for z_*, we obtain

$$z_* = \frac{\lambda_\alpha+\lambda_\beta \pm \sqrt{(\lambda_\alpha-\lambda_\beta)^2+c^2}}{2},$$

which is clearly real valued. Thus p_* is on the real axis or the unit circle. This implies that $X^-(p)/p$ has a positive imaginary part on the arc $(\beta,\alpha)_{\text{arc}}$, and hence $X^+(p)/p$ is purely imaginary with a negative imaginary part on $(\beta,\alpha)_{\text{arc}}$. This, together with the fact that $dp/p = id\omega$ in polar coordinates, $p = e^{i\omega}$, implies that

$$F(\alpha,\beta) = 2\int_{\omega_\beta}^{\omega_\alpha} \sqrt{-(\cos\omega-\lambda_0)^2+(\lambda_\alpha-\lambda_0)^2}\,d\omega \geq 0. \tag{55}$$

Setting $y = \cos\omega$ in (55) gives us

$$F(\alpha,\beta) = 2\int_{2\lambda_0-\lambda_\alpha}^{\lambda_\alpha} \frac{-1}{\sqrt{1-y^2}}\sqrt{-(y-\lambda_0)^2+(\lambda_\alpha-\lambda_0)^2}\,dy\,. \tag{56}$$

Now, for fixed λ_0 with $\lambda_\alpha \leq \lambda_0 \leq 0$, we differentiate F with respect to λ_α:

$$\frac{\partial F}{\partial\lambda_\alpha} = 2(\lambda_\alpha-\lambda_0)\int_{\lambda_\alpha}^{2\lambda_0-\lambda_\alpha} \frac{dy}{\sqrt{1-y^2}\sqrt{-(y-\lambda_0)^2+(\lambda_\alpha-\lambda_0)^2}}\,. \tag{57}$$

Here the contributions from the endpoints vanish. Since $1-y^2 > 0$ and $-(y-\lambda_0)^2+(\lambda_\alpha-\lambda_0)^2 > 0$ for $y \in (\lambda_\alpha, 2\lambda_0-\lambda_\alpha)$, $\frac{\partial F}{\partial\lambda_\alpha} < 0$ for fixed λ_0. This implies that F is a monotone decreasing function of λ_α as λ_α increases from -1 to λ_0. Thus, for any given $-1 \leq \lambda_0 \leq 0$, F attains its maximum value $F^*(\lambda_0)$ when $\lambda_\alpha = -1$. Moreover,

$$\frac{\partial F^*}{\partial\lambda_0} = 2\int_{-1}^{2\lambda_0+1} \frac{1+y}{\sqrt{1-y^2}\sqrt{-(y-\lambda_0)^2+(-1-\lambda_0)^2}}\,dy > 0, \tag{58}$$

which implies that F^* is a monotone increasing function of λ_0 as λ_0 increases from -1 to 0. Setting $z_0 = i$, $\alpha = -1$, and $\beta = 1$ gives

$$F(-1,1) = \int_0^\pi 2\sqrt{1-(\cos\omega)^2}\, d\omega = 2\int_0^\pi \sin\omega\, d\omega = 4, \tag{59}$$

which is the maximum value of F subject to the constraint $\lambda_\alpha + \lambda_\beta = 2\lambda_0$. Clearly, the choice $\alpha = \beta = z_0$ is admissible and it minimizes F at $F = 0$, whence we conclude $F(\alpha,\beta) \in [0,4]$. □

Similar to the case for the KdV (see [8, 38]), introduce the variable

$$s = -\frac{\log \rho_0^2}{t}.$$

Restricting to $\operatorname{Re}\alpha + \operatorname{Re}\beta = 2\lambda_0$, with $\operatorname{Im}\alpha$, $\operatorname{Im}\beta \geq 0$, the expression

$$\int_\beta^\alpha \frac{1}{p^2}\sqrt{(p-\alpha)\left(p-\alpha^{-1}\right)(p-\beta)\left(p-\beta^{-1}\right)}^{+}\, dp = s \tag{60}$$

defines both $\alpha(s)$ and $\beta(s)$ since s is a monotone function of $\operatorname{Re}\alpha$ (or, equivalently, of $\arg\alpha$). We define the g-function to be

(61)

$$g(z) = \frac{1}{2}\int_{\beta(s)}^{z} \frac{\sqrt{(p-\alpha)\left(p-\alpha^{-1}\right)(p-\beta)\left(p-\beta^{-1}\right)}}{p^2}\, dp + \frac{1}{2}\int_{-1}^{\alpha(s)} \frac{\sqrt{(p-\alpha)\left(p-\alpha^{-1}\right)(p-\beta)\left(p-\beta^{-1}\right)}}{p^2}\, dp,$$

We choose the branch cut for $\sqrt{(z-\alpha)(z-\beta)\left(z-\alpha^{-1}\right)\left(z-\beta^{-1}\right)}$ to contain the circular arcs on the unit circle from β to α and α^{-1} to β. In order for g to be single-valued, it is necessary to add a branch cut on the arc connecting α and α^{-1}.

Lemma C.2. *The g-function given by* (61) *satisfies:*

(1)

$$g^+(z) - g^-(z) = \begin{cases} \displaystyle\int_{\beta(s)}^{z} \frac{1}{p^2}\sqrt{(p-\alpha)\left(p-\alpha^{-1}\right)(p-\beta)\left(p-\beta^{-1}\right)}^{+}\, dp, & z \in (\beta(s),\alpha(s))_{arc} \\ \displaystyle\int_{\beta(s)}^{\alpha(s)} \frac{1}{p^2}\sqrt{(p-\alpha)\left(p-\alpha^{-1}\right)(p-\beta)\left(p-\beta^{-1}\right)}^{+}\, dp, & z \in \left(\alpha(s),\alpha(s)^{-1}\right)_{arc} \\ \displaystyle\int_{\beta(s)^{-1}}^{z} \frac{1}{p^2}\sqrt{(p-\alpha)\left(p-\alpha^{-1}\right)(p-\beta)\left(p-\beta^{-1}\right)}^{+}\, dp, & z \in \left(\alpha(s)^{-1},\beta^{-1}(s)\right)_{arc} \\ 0, & \textit{otherwise.} \end{cases} \tag{62}$$

(2)

$$g^+(z) + g^-(z) = \begin{cases} \displaystyle\int_{-1}^{\alpha(s)} \frac{1}{p^2}\sqrt{(p-\alpha)\left(p-\alpha^{-1}\right)(p-\beta)\left(p-\beta^{-1}\right)}\, dp, & z \in (\beta(s),\alpha(s))_{arc} \\ \displaystyle\int_{-1}^{z} \frac{1}{p^2}\sqrt{(p-\alpha)\left(p-\alpha^{-1}\right)(p-\beta)\left(p-\beta^{-1}\right)}\, dp, & z \in \left(\alpha(s),\alpha(s)^{-1}\right)_{arc} \\ \displaystyle\int_{-1}^{\alpha(s)^{-1}} \frac{1}{p^2}\sqrt{(p-\alpha)\left(p-\alpha^{-1}\right)(p-\beta)\left(p-\beta^{-1}\right)}\, dp, & z \in \left(\alpha(s)^{-1},\beta^{-1}(s)\right)_{arc} \\ 2g(z), & \textit{otherwise.} \end{cases} \tag{63}$$

(3)

$$g(z) = \frac{1}{2}z - \lambda_0 \log z + \mathcal{O}\left(z^{-1}\right), \ \textit{as } z \to \infty. \tag{64}$$

(4) $g(z) - \frac{1}{2t}\theta(z)$ *is bounded.*

(5)

$$\rho_0^2 e^{t\left(g^+(z)-g^-(z)\right)} = 1, \ \textit{for } z \in \left(\alpha(s),\alpha(s)^{-1}\right)_{arc}. \tag{65}$$

Proof. As before, set $X(p) = \sqrt{(p-\alpha)\left(p-\alpha^{-1}\right)(p-\beta)\left(p-\beta^{-1}\right)}$, and let λ_α and λ_β denote the real parts of α and β, respectively. The properties (1) and (2) follow from contour integration and the fact that $X^+\left(p^{-1}\right) = \frac{X^+(p)}{p^2}$. To prove (3), we use

$$\sqrt{1-y} = 1 - \frac{1}{2}y - \frac{1}{8}y^2 + \mathcal{O}\left(y^3\right), \text{ as } y \to 0,$$

and the condition that $\lambda_\alpha + \lambda_\beta = 2\lambda_0$, to obtain

$$\frac{X(p)}{p^2} = p^{-2} - 2\lambda_0 p^{-1} + \left(1 - \tfrac{1}{2}(\lambda_\alpha - \lambda_\beta)^2\right) + 4\lambda_0\lambda_\alpha\lambda_\beta p + \mathcal{O}\left(p^2\right), \text{ as } p \to 0\,. \tag{66}$$

Also, for large p, we have

$$\frac{X(p)}{p^2} = 1 - 2\lambda_0 p^{-1} + \left(1 - \tfrac{1}{2}(\lambda_\alpha - \lambda_\beta)^2\right) p^{-2} + 4\lambda_0\lambda_\alpha\lambda_\beta p^{-3} + \mathcal{O}\left(p^{-4}\right), \text{ as } p \to \infty. \tag{67}$$

Setting $H(z) = \displaystyle\int_{\alpha(s)}^{z} \frac{X(p)}{p^2}\,dp$, integration gives us

$$\begin{aligned} H(z) &= -z^{-1} + C - 2\lambda_0 \log z + \left(1 - \tfrac{1}{2}(\lambda_\alpha - \lambda_\beta)^2\right) z + \mathcal{O}\left(z^2\right), \text{ as } z \to 0, \\ H(z) &= z - 2\lambda_0 \log z + C - \left(1 - \tfrac{1}{2}(\lambda_\alpha - \lambda_\beta)^2\right) z^{-1} + \mathcal{O}\left(z^{-2}\right), \text{ as } z \to \infty, \end{aligned} \tag{68}$$

for some complex constant C. Then $\lim_{z\to\infty} H(z) + H\left(z^{-1}\right) = 2C$, which implies, for large $|z|$, that

$$\begin{aligned} 2C &= \int_{\alpha(s)}^{z} \frac{X(p)}{p^2}\,dp + \int_{\alpha(s)}^{z^{-1}} \frac{X(p)}{p^2}\,dp = \int_{\alpha(s)}^{z} \frac{X(p)}{p^2}\,dp + \int_{z}^{\alpha(s)^{-1}} \frac{X(p)}{p^2}\,dp \\ &= -\int_{\alpha(s)^{-1}}^{\alpha(s)} \frac{X(p)}{p^2}\,dp = -2\int_{-1}^{\alpha(s)} \frac{X(p)}{p^2}\,dp. \end{aligned} \tag{69}$$

Therefore, $g(z) = \frac{1}{2}z - \lambda_0 \log z + \mathcal{O}\left(z^{-1}\right)$ as $z \to \infty$. (4) follows from the integral representation and the asymptotic expansion around $z = 0$ in (68). Finally, to prove (5), assume $z \in \left(\alpha(s), \alpha(s)^{-1}\right)_{\text{arc}}$,

$$\begin{aligned} -\frac{\log\rho_0^2}{t} &= \int_{\beta(s)}^{\alpha(s)} \frac{X^+(p)}{p^2}\,dp \\ -\log\rho_0^2 &= t\left(g^+(z) - g^-(z)\right) \\ e^{t\left(g^+(z) - g^-(z)\right)}\rho_0^2 &= 1. \end{aligned}$$

□

C.2. **Derivation of the collisionless shock scaling.** We have

$$\rho_0 = \sqrt{1 - \left(\frac{n}{t}\right)^2} = \sqrt{2}\sqrt{1 - \frac{n}{t}}\left(1 + \mathcal{O}\left(1 - \frac{n}{t}\right)\right), \quad \text{for} \quad \frac{n}{t} \sim 1.$$

As described in Appendix C.1, we choose $A = K(\alpha)$ and $B = K(\beta)$ (see (41) for the transformation K) by

$$-\frac{\log\rho_0^2}{t\rho_0^3} = -i\int_B^A \frac{\sqrt{(q-A)(q-B)\left(q+\bar{A}\right)\left(q+\bar{B}\right)}^{+}}{(\lambda_0 - i\rho_0 q)^2}\,dq. \tag{70}$$

Note that as $\lambda_0 \to -1$, $\rho_0 \to 0$ (i.e. $z_0 \to -1$), the integral on the right hand side converges provided that A and B converge to finite values. To ensure this, we enforce that

$$-\frac{\log\rho_0^2}{\rho_0^3 t} \to C, \quad \text{as } t \to \infty, \tag{71}$$

for some constant $C \in \mathbb{R}$. Let $n = t - \frac{\mu(t)}{2}$, with $\frac{\mu(t)}{t} \to 0$ as $t \to \infty$, so that

$$\rho_0 = \sqrt{\mu(t)}\left(1 + \mathcal{O}\left(\tfrac{\mu(t)}{t}\right)\right). \tag{72}$$

Then

$$-\frac{\log \rho_0^2}{\rho_0^3 t} \sim \frac{-\log\left(\frac{\mu(t)}{t}\right)}{t\left(\frac{\mu(t)}{t}\right)^{3/2}} \to C\,, \quad \text{as} \quad t\to\infty\,. \tag{73}$$

For this limit to exist, set $\mu(t) = C_1 t^{1/3}(\log t)^{2/3}$, $C_1 > 0$. Doing so yields

$$-\frac{-\log\left(\frac{\mu(t)}{t}\right)}{t\left(\frac{\mu(t)}{t}\right)^{3/2}} = \frac{\frac{2}{3}\log t - \frac{2}{3}\log(\log t) - \log C_1}{C_1^{3/2}\log t} \to \frac{2}{3C_1^{3/2}}, \quad \text{as} \quad t\to\infty\,, \tag{74}$$

as desired: In this limit, A and B in (70), tend to finite values. Therefore the scaling for the collisionless shock region is given by

$$n = t - C_1 t^{1/3}(\log t)^{2/3}. \tag{75}$$

C.3. **Computing the Toda g-function.** To compute g we first compute $\mathfrak{g}$ and use the relation $tg(z) = t\mathfrak{g}(z) + \frac{1}{2}\theta(z)$. It follows that $\mathfrak{g}'(z)$ solves the following RH problem

$$\mathfrak{g}'(z) + \mathfrak{g}'(z) = t^{-1}\theta'(z),\ z\in\Sigma_u\cup\Sigma_l, \tag{76}$$

$$\mathfrak{g}'(z) = \mathcal{O}(z^{-2}),\ \text{as } z\to\infty. \tag{77}$$

Furthermore, $\mathfrak{g}'(z)$ is a bounded function on $\mathbb{C}\setminus(\Sigma_u\cup\Sigma_l)$. We remark that imposing that (76) and that $\mathfrak{g}'(z)$ is a bounded function in the finite plane uniquely determines $\mathfrak{g}'(z)$ and (77) is a consequence of our choice of α and β.

We consider the function $\mathfrak{G}(k) = \mathfrak{g}(M(k))$, bounded in the finite plane, where $M(k) = \frac{k+i}{k-i}$ maps the real axis to the unit circle. Then $\mathfrak{G}'(k)$ solves

$$\mathfrak{G}'(k) + \mathfrak{G}'(k) = t^{-1}\theta'(M(k))M'(k),\ z\in(-B,-A)\cup(A,B), \tag{78}$$

$$\mathfrak{G}'(k) = \mathcal{O}((k-i)^2),\ \text{as } k\to i. \tag{79}$$

Here $A = M^{-1}(\alpha)$ and $B = M^{-1}(\beta)$. As in the case of $\mathfrak{g}'(z)$ the behavior at $k = i$ does not need to be imposed — the boundedness of $\mathfrak{G}'$ along with the jump condition (78) are enough to uniquely determine the function. Thus the numerical methodology in [22] applies directly to this situation and allows us to compute both $\mathfrak{G}'$ and $\mathfrak{G}$ to within machine precision, uniformly in the complex plane. Hence $\mathfrak{g}(z) = \mathfrak{G}\left(i\frac{z+1}{z-1}\right)$ can be computed accurately.

References

[1] M. J. Ablowitz, P. A. Clarkson, *Solitons, Nonlinear Evolution Equations and Inverse Scattering*, Cambridge University Press, New York, NY, 1991.

[2] M. J. Ablowitz, A. S. Fokas, *Complex Variables: Introduction and Applications*, Cambridge University Press, New York, NY, 2005.

[3] M. J. Ablowitz, H. Segur, *Solitons and the Inverse Scattering Transform*, SIAM, Philadelphia, PA, 1981.

[4] D. Bilman, I. Nenciu, On the evolution of scattering data under perturbations of the Toda lattice, `arXiv:1405.2310`

[5] K. Clancey, I. Gohberg. *Factorization of Matrix Functions and Singular Integral Operators*, Birkhauser Verlag, Boston, MA, 1981.

[6] P. Deift, *Orthogonal Polynomials and Random Matrices: A Riemann-Hilbert Approach*, New York University Press, New York, NY, 1999.

[7] P. Deift, S. Kamvissis, T. Kriecherbauer, and X. Zhou, The Toda rarefaction problem, *Comm. Pure Appl. Math.* **49**, no. 1, 35–83 (1996).

[8] P. Deift, S. Venakides, X. Zhou, The collisionless shock region for the long-time behavior of solutions to the KdV equation, *Comm. Pure Appl. Math.* **47** (1994), 199–206.

[9] P. Deift, X. Zhou, A steepest descent method for oscillatory Riemann-Hilbert problems. Asymptotics for the MKdV equation, *Ann. Math.* **137** (1993), 295–368.

[10] P. Deift, X. Zhou, Asymptotics for the Painlevé II equation, *Comm. Pure Appl. Math.* **48** (1995), no.3, 277–337.

[11] P. Deift, X. Zhou, Perturbation theory for infinite-dimensional integrable systems on the line. A case study, *Acta. Math.* **188** (2002), 163–262.

[12] P. Deift, X. Zhou, S. Venakides, An extension of the steepest descent method for Riemann–Hilbert problems: the small dispersion limit of the Korteweg–de Vries equation, *Proc. Natl. Acad. Sci.*, **95**(2) (1998), :45–454

[13] H. Flaschka, The Toda lattice. I Existence of integrals, *Phys. Rev. B. (3)* **9** (1974), 1924–1625.
[14] H. Flaschka, The Toda lattice. II Inverse-scattering solution, *Progr. Theoret. Phys.* **51** (1974), 703–716.
[15] E. Fermi, J. Pasta, S. Ulam, *Studies of nonlinear problems. Collected Works of Enrico Fermi* Vol. II, pp. 978–988, University of Chicago Press, Chicago,1965.
[16] S. Kamvissis, On the long time behavior of the doubly infinite Toda lattice under initial data decaying at infinity, *Commun. Math. Phys.*, 153 479–t519, 1993.
[17] H. Krüger, G. Teschl, Long-time asymptotics for the Toda lattice in the soliton region, *Math. Z.* **262** (2009), 585–602.
[18] H. Krüger, G. Teschl, Long-time asymptotics of the Toda lattice for decaying initial data revisited, *Rev. Math. Phys.* **21** (2009), 61–109.
[19] N. I. Muskelishvili, *Singular Integral Equations*, Noordoff, Groningen, 1953.
[20] F. W. J. Olver, D. W. Lozier, R. F. Boisvert, and C. W. Clark, *NIST Handbook of Mathematical Functions*, Cambridge University Press, NY, 2010.
[21] S. Olver, A general framework for solving Riemann-Hilbert problems numerically, *Numer. Math.* **122**, 305–340, 2012.
[22] S. Olver, Computation of equilibrium measures, *J. Approx. Theory* **163**, 1185–1207, 2011.
[23] S. Olver, Computing the Hilbert transform and its inverse, *Math. Comput.* **80**, 1745–1767, 2011.
[24] S. Olver, Numerical solution of Riemann–Hilbert problems: Painlev II, *Found. Comput. Math* **11**, 153–179, 2010.
[25] S. Olver, *RHPackage*, `http://www.maths.usyd.edu.au/u/olver/projects/RHPackage.html`, 2011.
[26] S. Olver, T. Trogdon, Numerical Solution of Riemann–Hilbert Problems: Random Matrix Theory and Orthogonal Polynomials, *Constr. Approx.* **39**, 101–149, 2013.
[27] S. Olver, T. Trogdon, Nonlinear steepest descent and the numerical solution of Riemann-Hilbert problems, *Comm. Pure Appl. Math.*, **67** (8), 2014.
[28] H. Segur and M. Ablowitz, Asymptotic solutions of nonlinear equations and a Painlevé transcendent, *Physica D*, 1–2:165–184, 1981.
[29] G. Teschl, On the spatial asymptotics of solutions of the Toda lattice, *Discrete Contin. Dyn. Syst.* **27** (2010), no. 3, 1233–1239.
[30] G. Teschl, *Jacobi Operators and Completely Integrable Nonlinear Lattices*, Mathematical Surveys and Mono- graphs **72**, American Mathematical Society, Rhode Island (1999).
[31] M. Toda, *Theory of Nonlinear Lattices*, second edition, Springer Series in Solid-State Sciences, **20**, Springer-Verlag, Berlin, 1989.
[32] M. Toda, Vibration of a chain with nonlinear interaction, *J. Phys. Soc. Japan* **22**, 431–436, 1967.
[33] T. Trogdon, *Riemann–Hilbert Problems, Their Numerical Solution and the Computation of Nonlinear Special Functions*, PhD thesis, University of Washington, 2013.
[34] T. Trogdon, On the application of GMRES to oscillatory singular integral equations, *BIT Numer. Math.*, to appear, 2014.
[35] T. Trogdon and B. Deconinck, A numerical dressing method for the nonlinear superposition of solutions of the KdV equation, *Nonlinearity* **27**, 67–86, 2014.
[36] T. Trogdon and S. Olver, *Riemann–Hilbert Problems, Their Numerical Solution and the Computation of Nonlinear Special Functions*, SIAM, Philadelphia, PA, to appear.
[37] T. Trogdon and S. Olver, A Riemann–Hilbert approach to Jacobi operators and Gaussian quadrature, *IMA J. Numer. Anal.*, to appear, 2015.
[38] T. Trogdon, S. Olver, B. Deconinck, Numerical inverse scattering for the Korteweg-de Vries and modified Korteweg-de Vries equations, *Phys. D* **241** (2012), no. 11, 1003–1025.
[39] T. Trogdon, S. Olver, Numerical inverse scattering for the focusing and defocusing nonlinear Schrödinger equations. *Proc. R. Soc. A*, 469(2149), 2013.
[40] J. A. C. Weideman and L. N. Trefethen, The kink phenomenon in Fejér and Clenshaw–Curtis quadrature, *Numer. Math.* **107**, 707–727, 2007.
[41] X. Zhou, *Riemann-Hilbert problems and integrable systems*, Lectures at MSRI, 1999.

Deniz Bilman, Department of Mathematics, Statistics, and Computer Science, University of Illinois at Chicago, 851 S. Morgan Street, Chicago, IL 60607
E-mail address: `dbilma2@uic.edu`

Thomas Trogdon, Courant Institute of Mathematical Sciences, 251 Mercer Street, New York, NY 10012
E-mail address: `trogdon@cims.nyu.edu`